Measurement of B^0, B^0_s, B^+ and Λ^0_b production asymmetries in 7 and 8 TeV proton-proton collisions

Citation for published version:
Clarke, P, Cowan, G, Eisenhardt, S, Muheim, F, Needham, M, Playfer, S & Collaboration, LHC 2017, 'Measurement of B^0, B^0_s, B^+ and Λ^0_b production asymmetries in 7 and 8 TeV proton-proton collisions' Physics Letters B, vol. B774, Aaij:2017mso, pp. 139-158. DOI: 10.1016/j.physletb.2017.09.023

Digital Object Identifier (DOI):
10.1016/j.physletb.2017.09.023

Link:
Link to publication record in Edinburgh Research Explorer

Document Version:
Publisher's PDF, also known as Version of record

Published In:
Physics Letters B

Physics Letters B 774 (2017) 139–158

Contents lists available at ScienceDirect

Physics Letters B

www.elsevier.com/locate/physletb

Measurement of B^0, B_s^0, B^+ and Λ_b^0 production asymmetries in 7 and 8 TeV proton–proton collisions

LHCb Collaboration

ARTICLE INFO

Article history:
Received 10 April 2017
Received in revised form 5 September 2017
Accepted 11 September 2017
Available online xxxx
Editor: L. Rolandi

ABSTRACT

The B^0, B_s^0, B^+ and Λ_b^0 hadron production asymmetries are measured using a data sample corresponding to an integrated luminosity of 3.0 fb^{-1}, collected by the LHCb experiment in proton–proton collisions at centre-of-mass energies of 7 and 8 TeV. The measurements are performed as a function of transverse momentum and rapidity of the b hadrons within the LHCb detector acceptance. The overall production asymmetries, integrated over transverse momentum and rapidity, are also determined.

1. Introduction

The production rates of b and $\bar{b}$ hadrons are not expected to be identical in proton–proton collisions, as b and $\bar{b}$ quarks, produced in a hard scattering at the partonic level, might have different probabilities for coalescing with u or d valence quarks from the beam remnant. As a consequence, the production rates of B^+ and B^0 mesons may exceed those of B^- and $\overline{B}^0$, and b baryons can be produced more abundantly than $\bar{b}$ baryons. In the case of B_s^0 and $\overline{B}_s^0$ the production rates depend on the values of the other production asymmetries as no valence strange quark is present within the colliding protons and b and $\bar{b}$ quarks are predominantly produced in pairs.

The LHCb detector, thanks to its unique geometry as a forward spectrometer, is particularly suited to measure such asymmetries, as they are expected to be enhanced at forward rapidities and small transverse momenta. Other subtle effects of quantum chromodynamics, beyond the coalescence of b quarks and light valence quarks, may also contribute [1–3].

The measurements of hadron production asymmetries are of primary importance, not only for the understanding of the production mechanisms, but also for enabling precise measurements of *CP* violation in c and b hadrons at the LHC. Indeed, observed asymmetries must be corrected for production effects to obtain the *CP* asymmetries in the decays. Simulations that model the non-perturbative fragmentation of b quarks in proton–proton collisions at LHC energies predict asymmetries generally up to a few percent [4,5]. Production asymmetries of B^0 and B_s^0 mesons have been measured by LHCb at a centre-of-mass energy of 7 TeV, excluding values larger than a few percent [6]. The LHCb collaboration has also searched for possible production asymmetries for D^+ and D_s^+ mesons, finding the integrated D^+ production asymmetry different from zero at approximately three standard deviations [7,8]. In the b-baryon sector, the LHCb collaboration measured the sum of the Λ_b^0–$\overline{\Lambda}_b^0$ production asymmetry and the *CP* asymmetry in the $\Lambda_b^0 \to J/\psi\, pK^-$ decay [9], finding evidence for a dependence on Λ_b^0 rapidity.

This paper reports measurements of the production asymmetries, $A_{\mathrm{P}}\left(B^+\right)$, $A_{\mathrm{P}}\left(B^0\right)$ and $A_{\mathrm{P}}\left(B_s^0\right)$, measured using $B^+ \to J/\psi\, K^+$, $B^0 \to J/\psi\, K^{*0}$ and $B_s^0 \to D_s^- \pi^+$ decays. In addition, a measurement of $A_{\mathrm{P}}\left(\Lambda_b^0\right)$, determined indirectly from the other asymmetries, is presented. Hereafter, K^{*0} is used to refer to the $K^*(892)^0$ and the inclusion of charge-conjugate decay modes is implied throughout, except when referring to the production asymmetries, which are defined as

$$A_{\mathrm{P}}(x) \equiv \frac{\sigma\left(\bar{x}\right) - \sigma\left(x\right)}{\sigma\left(\bar{x}\right) + \sigma\left(x\right)}, \quad \text{with} \quad x \in \{B^+, B^0, B_s^0, \overline{\Lambda}_b^0\},$$

where σ denotes the inclusive production cross-section in a given region of phase space. The data sample, collected by LHCb in proton–proton collisions, corresponds to an integrated luminosity of 1.0 fb^{-1} at a centre-of-mass energy of 7 TeV, and 2.0 fb^{-1} at 8 TeV. The measurements are performed as a function of both the component of the momentum transverse to the beam (p_{T}) and the rapidity (y) of the hadrons within the LHCb detector acceptance, and are then integrated over the ranges $0 < p_{\mathrm{T}} < 30\ \text{GeV}/c$ and/or $2.1 < y < 4.5$ for B^+ and B^0 decays, and $2 < p_{\mathrm{T}} < 30\ \text{GeV}/c$ and/or $2.1 < y < 4.5$ for B_s^0 and Λ_b^0 decays. The ranges in p_{T} are not identical due to different trigger requirements between decays with and without muons in the final states. This analysis improves the previous one performed on B^0 and B_s^0 production asymmetries [6], using a larger data sample and a finer binning scheme for investigating the dependence on p_{T} and y. In addition, new

http://dx.doi.org/10.1016/j.physletb.2017.09.023

measurements of B^+ and Λ_b^0 production asymmetries have been included. Unlike in the previous analysis, the $B^0 \to D^-\pi^+$ decay is not considered, as it has been found not to improve the precision on the B^0 measurement.

2. Detector, trigger and simulation

The LHCb detector [10] is a single-arm forward spectrometer covering the pseudorapidity range $2 < \eta < 5$, designed for the study of particles containing b or c quarks. The detector includes a high-precision tracking system consisting of a silicon-strip vertex detector surrounding the proton–proton interaction region, a large-area silicon-strip detector located upstream of a dipole magnet with a bending power of about 4 Tm, and three stations of silicon-strip detectors and straw drift tubes placed downstream of the magnet.

The tracking system provides a measurement of momentum, p, of charged particles with a relative uncertainty that varies from 0.5% at low momentum to 1.0% at 200 GeV/c. The minimum distance of a track to a primary vertex (PV), the impact parameter (IP), is measured with a resolution of $(15 + 29/p_{\mathrm{T}})$ μm, where p_{T} is measured in GeV/c. Different types of charged hadrons are distinguished using information from two ring-imaging Cherenkov detectors. Photons, electrons and hadrons are identified by a calorimeter system consisting of scintillating-pad and preshower detectors, an electromagnetic calorimeter and a hadronic calorimeter. Muons are identified by a system composed of alternating layers of iron and multiwire proportional chambers. The trigger [11] consists of a hardware stage, based on information from the calorimeter and muon systems, followed by a software stage, which applies a full event reconstruction.

For $B^+ \to J/\psi K^+$ and $B^0 \to J/\psi K^{*0}$ decays, the data are collected by using the hardware muon trigger, which requires a single muon with large transverse momentum (from $p_{\mathrm{T}} > 1.4$ GeV/c to $p_{\mathrm{T}} > 1.8$ GeV/c) or a pair of muons with a large product of their transverse momenta (from $\sqrt{p_{\mathrm{T},1}\, p_{\mathrm{T},2}} > 1.3$ GeV/c to $\sqrt{p_{\mathrm{T},1}\, p_{\mathrm{T},2}} > 1.6$ GeV/c), depending on the data-taking conditions. For $B_s^0 \to D_s^-\pi^+$ decays, data are collected using the hadronic hardware trigger, which requires at least one cluster in the hadronic calorimeter with a transverse energy greater than 3.5 GeV or 3.7 GeV, depending on the data-taking period. The output is then processed by the software trigger. In the case of $B^+ \to J/\psi K^+$ and $B^0 \to J/\psi K^{*0}$ decays, J/ψ mesons consistent with coming from the decay of a b-hadron are selected by requiring that their decay products form a displaced vertex and have large IPs at the PV with respect to which the B candidate has the smallest χ^2_{IP}. The quantity χ^2_{IP} is defined as the difference in the vertex-fit χ^2 of a given PV reconstructed with and without the particle under consideration. The $B_s^0 \to D_s^-\pi^+$ decays are selected by requiring a two- or three-track secondary vertex with a significant displacement from all PVs. At least one charged particle must have a transverse momentum $p_{\mathrm{T}} > 1.7$ GeV/c and be inconsistent with originating from a PV. A multivariate algorithm [12] is used for the identification of secondary vertices consistent with the decay of a b hadron.

Simulated events are used to determine the signal selection efficiency as a function of p_{T} and y, and to study the modelling of the decay-time resolution, the reconstruction efficiency as function of the decay time and the shape of the invariant mass distribution of partially reconstructed background. In the simulation, proton–proton collisions are generated using Pythia [13,4] with a specific LHCb configuration [14]. Decays of hadronic particles are described by EvtGen [15], in which final-state radiation is generated using Photos [16]. The interaction of the generated particles with the detector, and its response, are implemented using the Geant4 toolkit [17,18] as described in Ref. [19].

3. Methodology

The asymmetries $A_{\mathrm{P}}(B^0)$ and $A_{\mathrm{P}}(B_s^0)$ are measured by means of a time-dependent analysis of $B^0 \to J/\psi K^{*0}$ decays, with $J/\psi \to \mu^-\mu^+$ and $K^{*0} \to K^-\pi^+$, and $B_s^0 \to D_s^-\pi^+$ decays, with $D_s^- \to K^+K^-\pi^-$. The decay rate to a flavour-specific final state f of a $B^0_{(s)}$ meson with average decay width $\Gamma_{d(s)}$ can be written as

$$S(t,\psi,\xi) \propto (1-\psi A_{CP})(1-\psi A_{\mathrm{D}}) \\ e^{-\Gamma_{d(s)}t}\left[\Omega_+^{\xi}\cosh\left(\frac{\Delta\Gamma_{d(s)}t}{2}\right) + \psi\,\Omega_-^{\xi}\cos\left(\Delta m_{d(s)}t\right)\right], \tag{1}$$

where $\Delta m_{d(s)} \equiv m_{d(s),\,\mathrm{H}} - m_{d(s),\,\mathrm{L}}$ and $\Delta\Gamma_{d(s)} \equiv \Gamma_{d(s),\,\mathrm{L}} - \Gamma_{d(s),\,\mathrm{H}}$ are the mass and width differences of the $B^0_{(s)}$–$\overline{B}^0_{(s)}$ system mass eigenstates. The subscripts H and L denote the heavy and light eigenstates, respectively. The symbol ψ is the tag of the final state, which assumes the values $\psi = 1$ if the final state is f and $\psi = -1$ if the final state is the CP conjugate $\bar{f}$, while ξ indicates the tag of the initial flavour of the $B^0_{(s)}$ meson, which takes the values $\xi = 1$ for $B^0_{(s)}$ and $\xi = -1$ for $\overline{B}^0_{(s)}$. The terms Ω_+^{ξ} and Ω_-^{ξ} are defined as

$$\Omega_{\pm}^{\xi} \equiv \delta_{+1\xi}\,(1-A_{\mathrm{P}})\left|\frac{q}{p}\right|^{1-\psi} \pm \delta_{-1\xi}\,(1+A_{\mathrm{P}})\left|\frac{q}{p}\right|^{-1-\psi},$$

where p and q are complex parameters entering the definition of the two mass eigenstates of the effective Hamiltonian of the $B^0_{(s)}$ system, $|B_{\mathrm{H}}\rangle = p|B^0_{(s)}\rangle - q|\overline{B}^0_{(s)}\rangle$ and $|B_{\mathrm{L}}\rangle = p|B^0_{(s)}\rangle + q|\overline{B}^0_{(s)}\rangle$, and δ_{ij} is the Kronecker delta. The symbol A_{D} represents the detection asymmetry of the final state, defined in terms of the f and $\bar{f}$ detection efficiencies, ε, as

$$A_{\mathrm{D}} \equiv \frac{\varepsilon_{\bar{f}} - \varepsilon_f}{\varepsilon_{\bar{f}} + \varepsilon_f}.$$

The direct CP asymmetry A_{CP} is defined as

$$A_{CP} \equiv \frac{\mathcal{B}\left(\overline{B}^0_{(s)} \to \bar{f}\right) - \mathcal{B}\left(B^0_{(s)} \to f\right)}{\mathcal{B}\left(\overline{B}^0_{(s)} \to \bar{f}\right) + \mathcal{B}\left(B^0_{(s)} \to f\right)}$$

where the symbol $\mathcal{B}$ stands for the branching fraction of the decay considered.

The asymmetry $A_{\mathrm{P}}(B^+)$ is measured by means of a time-integrated analysis of $B^+ \to J/\psi K^+$ decays, with $J/\psi \to \mu^+\mu^-$, starting from the raw asymmetry defined as

$$A_{\mathrm{raw}} \equiv \frac{N(B^- \to J/\psi K^-) - N(B^+ \to J/\psi K^+)}{N(B^- \to J/\psi K^-) + N(B^+ \to J/\psi K^+)},$$

where N denotes the observed yields. The raw asymmetry can be written, up to $\mathcal{O}(10^{-6})$ corrections, as

$$A_{\mathrm{raw}} = A_{\mathrm{P}}(B^+) + A_{\mathrm{D}}(K^+) + A_{CP}(B^+ \to J/\psi K^+), \tag{2}$$

where $A_{\mathrm{D}}(K^+)$ is the K^+ detection asymmetry, measured by means of charm control samples as in Ref. [20], and $A_{CP}(B^+ \to J/\psi K^+)$ is the CP asymmetry in the decay, measured by BaBar, Belle and D0 [21–23]. An improved measurement of the CP asymmetry was also made recently by LHCb [24], using an independent data sample selected with different trigger requirements. The A_{P} values obtained from Eq. (1) and Eq. (2) are detector-independent quantities only if measured in kinematic regions where the reconstruction efficiencies are constant. To account for the dependence of the production asymmetries on the kinematics of the B^+, B^0 and B_s^0 mesons, each data sample is divided into bins of (p_{T}, y), and the measurement is performed for each bin. Fig. 1 shows

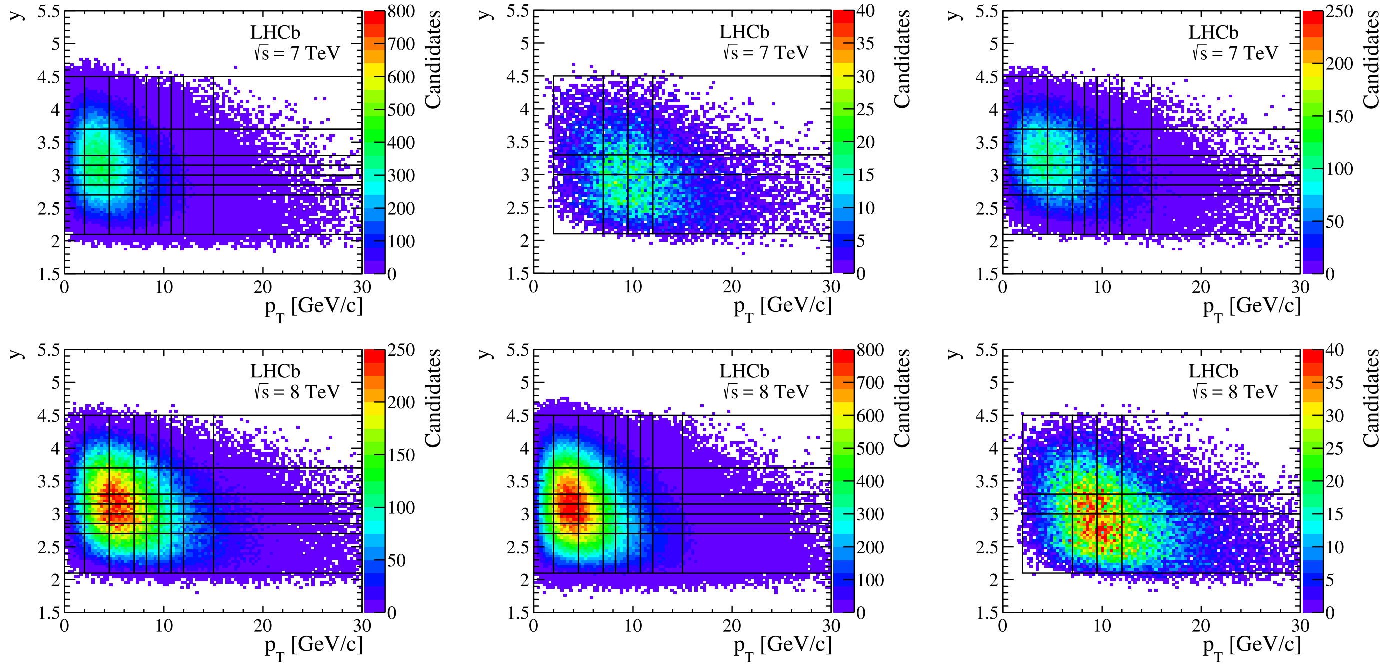

Fig. 1. Distributions of p_T and y for background-subtracted (left) B^+, (middle) B^0 and (right) B^0_s decays for data collected in proton–proton collisions at the centre-of-mass energies of (top) 7 and (bottom) 8 TeV. The binning schemes are superimposed.

the distribution of (p_T, y) for $B^+ \to J/\psi K^+$, $B^0 \to J/\psi K^{*0}$ and $B^0_s \to D^-_s \pi^+$ decays, where the background components are subtracted using the *sPlot* technique [25] and the definition of the various kinematic bins is overlaid. For the B^+ and B^0 decays a common set of bins is used, defined in Table 6 of the Appendix, and in the case of the B^0_s decay, the binning scheme is reported in Table 8.

In proton–proton collisions at the LHC, b and $\bar{b}$ quarks are predominantly pair-produced via strong interaction processes. This leads to a relation between the Λ^0_b production asymmetry and the other b-hadron production asymmetries, namely

$$A_P(\Lambda^0_b) = -\left[\frac{f_u}{f_{\Lambda^0_b}} A_P(B^+) + \frac{f_d}{f_{\Lambda^0_b}} A_P(B^0)\right.$$

$$\left. + \frac{f_s}{f_{\Lambda^0_b}} A_P(B^0_s) + \frac{f_c}{f_{\Lambda^0_b}} A_P(B^+_c) + \frac{f_{\text{other}}}{f_{\Lambda^0_b}} A_P(\text{other})\right],$$

where f_u, f_d, f_s, f_c, $f_{\Lambda^0_b}$ and f_{other} are the fragmentation fractions of a b quark hadronizing into weakly-decaying B^+, B^0, B^0_s, B^+_c mesons, Λ^0_b baryons and all the other b-baryon species. The ratios of the fragmentation fractions, $f_u/f_{\Lambda^0_b}$, $f_d/f_{\Lambda^0_b}$ and $f_s/f_{\Lambda^0_b}$ are taken from LHCb measurements reported in Refs. [26,27]. Their dependence on p_T and y is taken into account. The terms $(f_c/f_{\Lambda^0_b}) \cdot A_P(B^+_c)$ and $(f_{\text{other}}/f_{\Lambda^0_b}) \cdot A_P(\text{other})$ are of the order of $3 \cdot 10^{-5}$ and $2 \cdot 10^{-3}$, respectively. This is estimated assuming that the value of $A_P(B^+_c)$ and $A_P(\text{other})$ are of the same order as the B-meson production asymmetries ($\simeq 10^{-2}$) and taking the values of $f_c/f_{\Lambda^0_b}$ and $f_{\text{other}}/f_{\Lambda^0_b}$ from simulation. Neglecting these terms, the Λ^0_b production asymmetry can be measured using the approximate relation

$$A_P(\Lambda^0_b) \simeq -\left[\frac{f_u}{f_{\Lambda^0_b}} A_P(B^+) + \frac{f_d}{f_{\Lambda^0_b}} A_P(B^0) + \frac{f_s}{f_{\Lambda^0_b}} A_P(B^0_s)\right]. \qquad (3)$$

Possible small deviations from this approximation, due in particular to contributions from other b baryons, are taken into account in the evaluation of systematic uncertainties.

3.1. Integrated production asymmetries

In addition to the measurements in bins, integrated production asymmetries, where efficiency corrections have been applied, are also provided. The integration of the A_P values is performed in the ranges $0 < p_T < 30$ GeV/c and $2.1 < y < 4.5$ for the B^+ and B^0 decays and in the ranges $2 < p_T < 30$ GeV/c and $2.1 < y < 4.5$ for the B^0_s and Λ^0_b decays. The integrated value of A_P is given by

$$A_P = \sum_i \frac{N_i}{\varepsilon_i} A_{P,i} \Big/ \sum_i \frac{N_i}{\varepsilon_i} \qquad (4)$$

where the index i runs over the bins, N_i is the number of observed signal events in the i-th bin and ε_i is the efficiency defined as the number of selected events divided by the number of produced events in the i-th bin. The signal yield in each bin can be expressed as

$$N_i = \mathcal{L}\, \sigma_{b\bar{b}}\, 2\, f_q\, \mathcal{B}\, F_i\, \varepsilon_i \qquad (5)$$

where $\mathcal{L}$ is the integrated luminosity, $\sigma_{b\bar{b}}$ is the $b\bar{b}$ cross section, f_q is the fragmentation fraction for quark flavour q, with $q \in \{u, d, s\}$, F_i stands for the fraction of the b hadrons produced in the i-th bin and $\mathcal{B}$ is the branching fraction of the b-hadron decay being considered. By substituting N_i/ε_i from Eq. (5) into Eq. (4), the integrated value of A_P becomes

$$A_P = \sum_i \omega_i A_{P,i},$$

where $\omega_i = F_i / \sum_i F_i$. The ω_i values are determined using simulated events, generated with proton–proton collisions at the centre-of-mass energies of 7 and 8 TeV.

4. Data set and event selections

The selections of $B^+ \to J/\psi K^+$ and $B^0 \to J/\psi K^{*0}$ decays are based on the reconstruction of $J/\psi \to \mu^-\mu^+$ decays combined with either a track identified as a kaon or with a K^{*0} decaying to $K^+\pi^-$. The J/ψ candidates are formed from two oppositely charged tracks originating from a common vertex, identified as muons with $p_{\mathrm{T}} > 500$ MeV/c. The K^{*0} candidates are formed from two oppositely charged tracks, one identified as a kaon and the other as a pion, originating from the same vertex. They are required to have $p_{\mathrm{T}} > 1$ GeV/c and the $K^+\pi^-$ invariant mass in the range 826–966 MeV/c^2. The invariant mass of B^0 and B^+ candidates, calculated constraining the two muon candidates to have the known J/ψ mass, is required to be in the range 5150–5450 MeV/c^2. The proper decay time of the B-meson candidate is calculated from a fit that constrains the candidate to originate from the PV with the smallest χ^2_{IP} with respect to the B candidate. Only B-meson candidates with a decay time greater than 0.2 ps are retained. This lower bound on the decay time rejects a large fraction of the combinatorial background.

In the case of $B_s^0 \to D_s^-\pi^+$ decays, the D_s^- candidates are reconstructed using the $K^+K^-\pi^-$ decay channel. Requirements are applied to the D_s^- decay products before combining them to form a common vertex, namely the scalar p_{T} sum of the tracks must exceed 1.8 GeV/c and the largest distance of closest approach between all possible pairs of tracks must be less than 0.5 mm. The D_s^- candidates are then required to be significantly detached from the PV and to have the invariant mass within the range 1949–1989 MeV/c^2. Each D_s^- candidate is subsequently combined with a second charged pion, referred to as the accompanying pion in the following, to form the B-meson decay vertex. The sum of the p_{T} values of the D_s^- and accompanying π^+ must be larger than 5 GeV/c and the decay time of B-meson candidates must be greater than 0.2 ps. Furthermore, the cosine of the angle between the B-meson candidate momentum vector and the vector connecting the PV and B-meson candidate vertex is required to be larger than 0.999.

Stringent particle identification criteria are required to be satisfied for the kaons and pions forming the K^{*0} and D_s^- candidates, the kaon from the B^+ decay and the accompanying pion, in order to reduce to a negligible level the background from other B-meson decays with a misidentified kaon or pion, and from Λ_b^0 decays with a misidentified proton.

A final selection is applied using a multivariate analysis method based on a Boosted Decision Tree [28,29], where the variables used in the selection are: the p_{T} and the IP of the B decay products, the flight distance and the IP of the B candidate, and, in the case of B_s^0, the flight distance of the D_s^- meson. The multivariate selection is trained using simulated events as a proxy for the signal, and B-meson candidates from data selected in the upper mass sidebands to represent the background.

5. Fit model

For each signal and background component, the invariant mass distribution of all B candidates, and, in the case of $B^0_{(s)}$, the decay time, is modelled by defining appropriate probability density functions (PDFs). Two categories of background are considered: the combinatorial background, due to the random association of tracks, and the partially reconstructed background, due to decays with a topology similar to that of the signal, but with one or more particles not reconstructed. The latter is only relevant for $B_s^0 \to D_s^-\pi^+$ decays.

5.1. Invariant mass parameterization

The signal component for B mesons is modelled by convolving a sum of two Gaussian functions with a function parameterizing the final-state QED radiation (FSR). The PDF of the invariant mass, m, is given by the convolution

$$g(m) \propto \int_0^{+\infty} (m')^s G\left(m + m'; \mu\right) \mathrm{d}m' \tag{6}$$

where G is the sum of two Gaussian functions with different widths and common mean μ that represents the B-meson mass. The parameter s governs the amount of FSR, and using simulation is found to be $s = -0.9966 \pm 0.0005$ for the B^+ decay, $s = -0.9945 \pm 0.0003$ for the B^0 decay and $s = -0.9832 \pm 0.0004$ for the B_s^0 decay. The invariant mass shape of the combinatorial background is well described by an exponential PDF.

Regarding the $J/\psi K^+$ invariant mass spectrum, common parameters are used for both B^+ and B^- mesons. In the case of the $D_s^-\pi^+$ spectrum, a background component due to partially reconstructed B_s^0 decays is also present in the low invariant mass region. The contributions with the highest branching fractions are from the $B_s^0 \to D_s^{*-}\pi^+$ decay, with $D_s^{*-} \to D_s^-\gamma$ or $D_s^{*-} \to D_s^-\pi^0$, where the γ or π^0 is not reconstructed, and from the $B_s^0 \to D_s^-\rho^+$ decay, with $\rho^+ \to \pi^+\pi^0$, where the π^0 is not reconstructed. The partially reconstructed components are parameterized by means of a kernel estimation technique [30] based on invariant mass distributions obtained from simulated events, where the same selection applied to data is used and differences in invariant mass resolution between data and simulation are taken into account. The yields are obtained from the fits.

In the case of the $B_s^0 \to D_s^-\pi^+$ decay, an irreducible background component due to the $B^0 \to D_s^+\pi^-$ decay is also present. This component is accounted for in the fits using the same parameterization adopted for the signal, where the mean values of the two signal PDFs are separated by the difference in the known masses between B^0 and B_s^0 mesons [31] and the production asymmetry is fixed to the B^0 measured value. The yield of this component is fixed according to the known branching fraction [31].

5.2. Decay time parameterization

Starting from Eq. (1) and summing over ξ, the decay rate to a flavour-specific final state of a neutral B meson is parameterized by the convolution

$$S(t, \psi) \propto \left[1 - \psi\left(A_{CP} + A_D\right)\right] \Bigg\{ e^{-\Gamma_{d(s)} t} \left[\Lambda_+ \cosh\left(\frac{\Delta\Gamma_{d(s)} t}{2}\right) + \psi \Lambda_- \cos\left(\Delta m_{d(s)} t\right)\right] \otimes R(t) \Bigg\} \epsilon(t)\,, \tag{7}$$

where $R(t)$ is a function describing the decay-time resolution, as discussed in Sec. 5.3, and $\epsilon(t)$ is the reconstruction efficiency as a function of the decay time determined from simulation and parameterized for the B^0 decay by

$$\epsilon(t) = \frac{1}{2}\left[1 - \mathrm{erf}\left(p_1 t^{p_2}\right)\right](1 + p_3 t)\,,$$

and for the B_s^0 decay by

$$\epsilon(t) = \frac{1}{2}\left[1 - \frac{1}{2}\mathrm{erf}\left(\frac{n_1 - t}{t}\right) - \frac{1}{2}\mathrm{erf}\left(\frac{n_2 - t}{t}\right)\right](1 + n_3 t)\,,$$

where erf is the error function, and p_i and n_i are parameters determined from simulation. The terms Λ_+ and Λ_- are defined as

Table 1
Values of the various physical inputs used in the fits, as reported in Ref. [33].

Parameter	Value
Δm_d [ps^{-1}]	0.5065 ± 0.0019
Δm_s [ps^{-1}]	17.757 ± 0.021
Γ_d [ps^{-1}]	0.6579 ± 0.0017
Γ_s [ps^{-1}]	0.6645 ± 0.0018
$\Delta\Gamma_s$ [ps^{-1}]	0.083 ± 0.006
$\lvert q/p\rvert_{B^0}$	1.0007 ± 0.0009
$\lvert q/p\rvert_{B_s^0}$	1.0038 ± 0.0021

$$\Lambda_{\pm} \equiv (1 - A_{\mathrm{P}})\left|\frac{q}{p}\right|^{1-\psi} \pm (1 + A_{\mathrm{P}})\left|\frac{q}{p}\right|^{-1-\psi},$$

and the term $A_{CP}A_{\mathrm{D}}$ is neglected, as A_{D} is $\mathcal{O}(10^{-2})$ [32] and A_{CP} is very small for the decays under study. For this reason, it is only possible for the fit to determine the sum of A_{D} and A_{CP}, but not their individual values.

The decay-time PDF of the combinatorial background is studied using events from a high invariant mass window where the signal is not present, namely in the range 5310–5340 MeV/c^2 for $B^0 \to J/\psi K^{*0}$ and 5450–5900 MeV/c^2 for $B_s^0 \to D_s^-\pi^+$ decays. The partially reconstructed component for the $B_s^0 \to D_s^-\pi^+$ decay is determined from simulated events.

5.3. Decay time resolution

The decay-time resolutions of B^0 and B_s^0 mesons are estimated by studying the decay time of fake B candidates, formed from a D^- decaying to $K^+\pi^-\pi^-$ and a pion track, both coming from the same PV. These B candidates are called fake, as the probability to form a real decay with this technique is negligible. In order to avoid the introduction of biases in the decay-time measurements, the accompanying pion is selected with requirements on momentum and p_{T}, rather than on IP. The decay-time distribution of these fake B candidates yields an estimate of the decay-time resolution of a real decay. This method is verified by means of simulated events, both for signal and fake B decays. The resolution model, $R(t)$, consisting of a sum of three Gaussian functions with zero mean and three different widths, characterized by an average width of 49 fs, is used. The resolution is found to be overestimated by about 4 fs and to be dependent on the decay time. Taking these effects into account, an uncertainty of 8 fs on the average width is considered as a systematic uncertainty. It is estimated from simulation that the measurement of the decay time is biased by no more than 2 fs, and this effect is also accounted for as a systematic uncertainty.

6. Determination of the production asymmetries

The production asymmetries are determined by means of unbinned ($B^0_{(s)}$) and binned (B^+) maximum likelihood fits, for each kinematic bin, to the invariant mass (B^+) and invariant mass and decay time ($B^0_{(s)}$) distributions, using the models described in the previous section. The models are validated with a series of fits to the mass and lifetime distributions of events obtained from pseudoexperiments. No evidence of biases on central values nor on the uncertainty is found. Furthermore, a global fit to the total sample of selected candidates is performed for each of the three decay modes to validate the fitting model on data. In the case of the time-dependent analysis, the mass differences Δm_d and Δm_s, the mixing parameters $|q/p|_{B^0}$ and $|q/p|_{B_s^0}$, the average decay widths Γ_d and Γ_s, and the width difference $\Delta\Gamma_s$ are fixed to the central values of the measurements reported in Table 1. The width difference $\Delta\Gamma_d$ is fixed to zero.

As already mentioned, for small values of A_{CP} and A_{D}, the decay rate is to first order only sensitive to the sum of these two quantities. For this reason, A_{CP} is fixed to zero and A_{D} is left as a free parameter in the fits and hence measured from data, oppositely to the B^+ case, where an external input is necessary for A_{D}. It is verified that the choice of different A_{CP} values, up to the few percent level, leads to negligible variations of A_{P}. Figs. 2 and 3 show the $J/\psi K^+$, $J/\psi K^+\pi^-$ and $D_s^-\pi^+$ invariant mass distributions and, in the case of the neutral B meson, the time distributions with the results of the global fits overlaid, for data recorded at centre-of-mass energies of 7 and 8 TeV.

Fig. 4 shows the raw asymmetries for neutral B-meson decays, defined as the ratio between the difference and the sum of the overall decay-time distributions, as a function of the decay time for candidates in the signal invariant mass regions, defined as the ranges 5250–5310 MeV/c^2 for B^0 decay and 5290–5450 MeV/c^2 for B_s^0 decay. The results of the global fits are overlaid.

The signal yields, A_{P} values and detection asymmetries obtained from the global fits are reported in Table 2, for the neutral B-meson decays, while the signal yield and A_{raw} for the B^+ decay are reported in Table 3. The A_{P} values obtained from the time-dependent global fits, reported here for illustrative purposes, are detector-independent quantities only if efficiency corrections as a function of p_{T} and y are applied. An accurate knowledge of the decay-time resolution is important for the $B_s^0 \to D_s^-\pi^+$ decay, due to the fast oscillation of the B_s^0 meson. For this reason the decay-time resolution is determined using the method previously described, applied to candidates in each (p_{T}, y) bin.

According to Eq. (2), the measurement of $A_{\mathrm{P}}(B^+)$ requires knowledge of the CP asymmetry $A_{CP}(B^+ \to J/\psi K^+)$ and $A_{\mathrm{D}}(K^+)$. The value recently measured by LHCb [24] with an independent data set is used for the former and corresponds to $A_{CP}(B^+ \to J/\psi K^+) = (0.09 \pm 0.27\ (\mathrm{stat}) \pm 0.07\ (\mathrm{syst})) \times 10^{-2}$. The measurement of the kaon detection asymmetry is obtained from D-meson decays produced directly in proton–proton collisions, using the same technique reported in Ref. [20]. It consists of measuring raw asymmetries from the two decay modes, $D^+ \to K^-\pi^+\pi^+$ and $D^+ \to K_{\mathrm{S}}^0\pi^+$ with $K_{\mathrm{S}}^0 \to \pi^+\pi^-$, to obtain the $K^+\pi^-$ detection asymmetry, $A_{\mathrm{D}}(K^+\pi^-)$, in each (p_{T}, y) bin of the B^+ mesons. Additionally, $A_{\mathrm{D}}(K^+)$ is obtained by subtracting from $A_{\mathrm{D}}(K^+\pi^-)$ the pion detection asymmetry, $A_{\mathrm{D}}(\pi^-)$, measured by means of a sample of partially and fully reconstructed $D^{*+} \to D^0(K^-\pi^+\pi^-\pi^+)\pi^+$ decays, as described in Ref. [8]. It is estimated that the pion detection asymmetries across the various B^+ meson bins of (p_{T}, y) are in the range 0–0.2 %. Finally, the detection asymmetry of the $K^0 \to \pi^+\pi^-$ final state, $A_{\mathrm{D}}(K^0)$, measured by LHCb to be $A_{\mathrm{D}}(K^0) = (0.054 \pm 0.014)\%$ [20], is also subtracted.

7. Systematic uncertainties

Several sources of systematic uncertainty are considered. They are evaluated for each kinematic bin and for each decay mode. For the invariant mass model, the effects of the uncertainty on the shapes of all components (signals, combinatorial and partially reconstructed backgrounds) are investigated. For the decay-time model, systematic effects related to the decay-time resolution and reconstruction efficiency are studied. The effects of the uncertainties on the external inputs used in the fits, reported in Table 1, are evaluated by repeating the fits with each parameter varied by ±1 standard deviation (σ). Alternative decay-time parameterizations of the background components are also considered. To estimate the contribution of each single source, the fit is repeated for each (p_{T}, y) bin after having modified the baseline fit model. The shifts

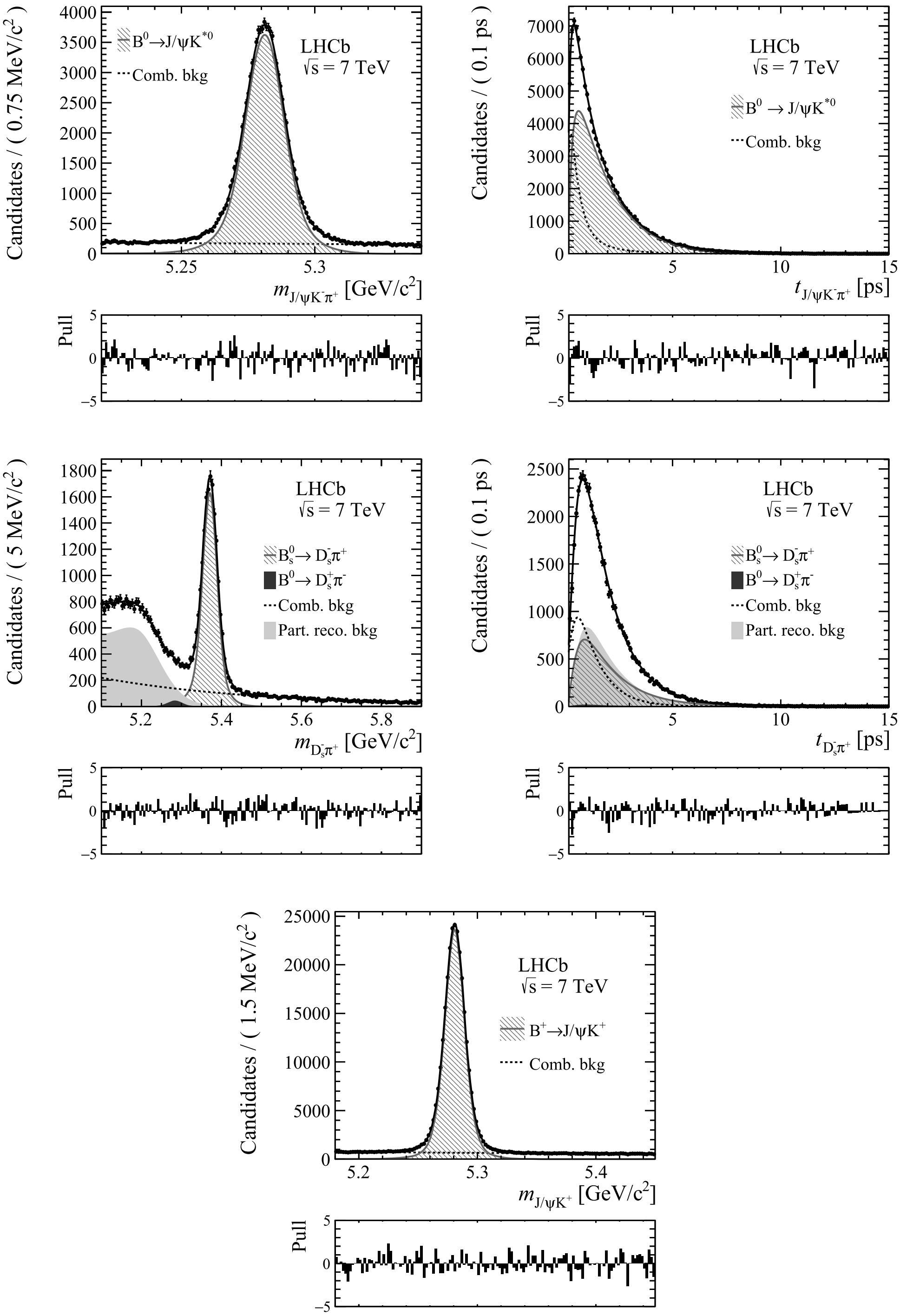

Fig. 2. Distributions of (left) invariant mass and (right) decay time for (top) $B^0 \to J/\psi K^{*0}$, (middle) $B_s^0 \to D_s^- \pi^+$ and (bottom) of invariant mass for $B^+ \to J/\psi K^+$ decays, with the results of the fit overlaid. The data were collected in proton–proton collisions at the centre-of-mass energy of 7 TeV. The contributions of the various background sources are also shown. Below each plot are the normalized residual distributions.

from the relevant baseline values are taken as the systematic uncertainties. A detailed description follows. To estimate a systematic uncertainty related to the parameterization of final-state radiation effects on the signal mass distributions, the parameter s of Eq. (6) is varied by $\pm 1\sigma$ of the corresponding value obtained from fits to simulated decays. A systematic uncertainty related to the invariant mass resolution model is estimated by repeating the fit using a simplified model with a single Gaussian function. The systematic uncertainty related to the parameterization of the mass distribution for the combinatorial background is investigated by replacing the exponential function with a linear function. Concerning the partially reconstructed background, a systematic uncertainty is assessed by repeating the fits while excluding the low invariant mass region, applying the requirement $m > 5330$ MeV/c^2 to $B_s^0 \to D_s^- \pi^+$ candidates. To estimate the uncertainty related to the parameterization of signal decay-time reconstruction efficiency, different functions are considered. Effects of inaccuracies in the knowledge of the decay-time resolution are estimated by rescaling

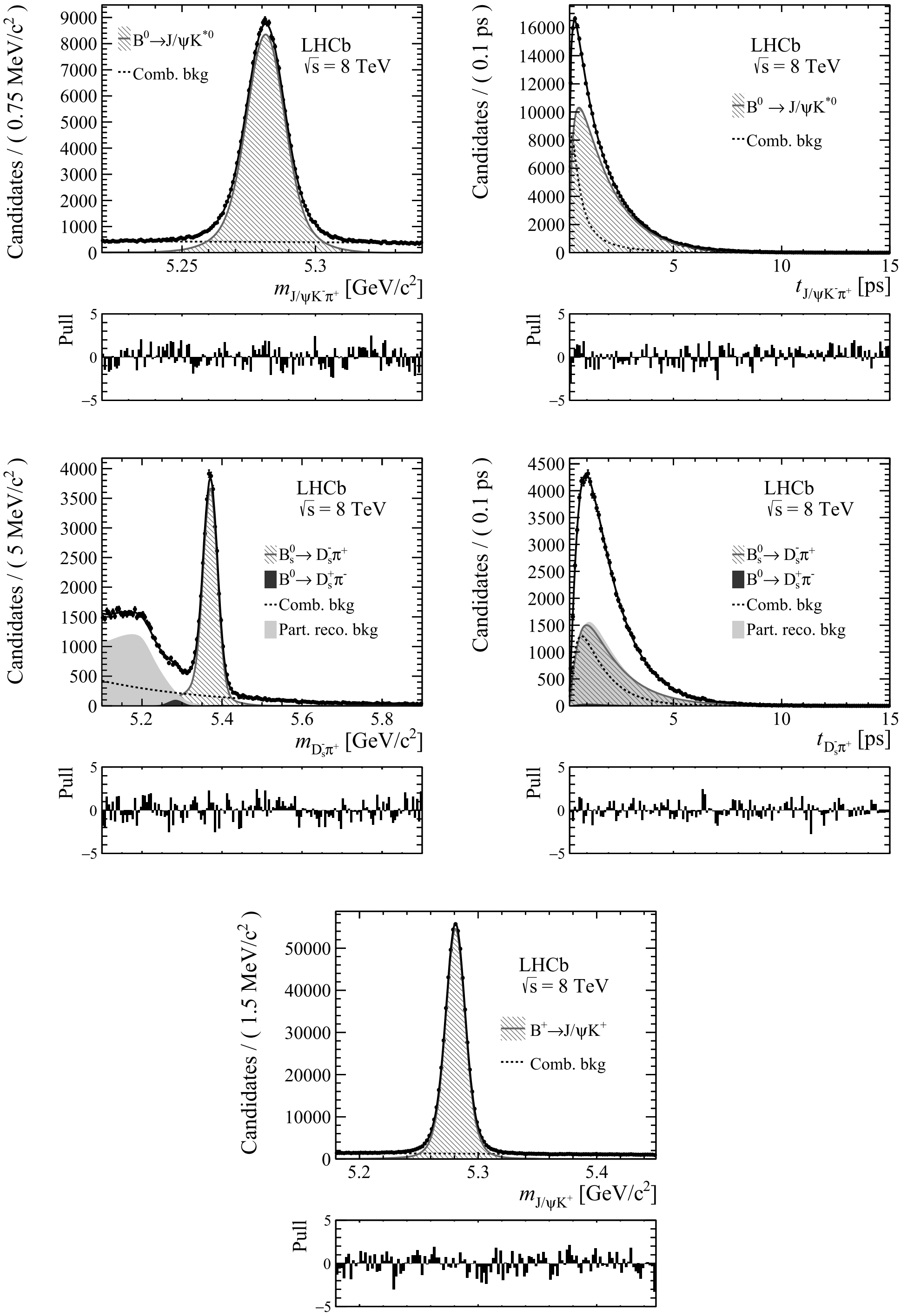

Fig. 3. Distributions of (left) invariant mass and (right) decay time for (top) $B^0 \to J/\psi K^{*0}$, (middle) $B_s^0 \to D_s^- \pi^+$ and (bottom) of invariant mass for $B^+ \to J/\psi K^+$ decays, with the results of the fit overlaid. The data were collected in proton–proton collisions at the centre-of-mass energy of 8 TeV. The contributions of the various background sources are also shown. Below each plot are the normalized residual distributions.

the widths of the baseline model to obtain an average resolution width differing by ±8 fs. The impact of the small bias in the reconstructed decay time is assessed by introducing a corresponding bias of ±2 fs in the decay-time resolution model. The determination of the systematic uncertainties related to the $|q/p|$ input values requires special treatment, as A_{P} is correlated with $|q/p|$. For this reason, any variation of $|q/p|$ produces the same shift of A_{P} in each of the kinematic bins. Such a correlation is taken into account when integrating over p_{T} and y. The values of the systematic uncertainties related to the knowledge of $|q/p|$ are 0.0009 in the case of $A_{\mathrm{P}}(B^0)$ and 0.0021 in the case of $A_{\mathrm{P}}(B_s^0)$. For the B^+ decay, the uncertainties on $A_{CP}(B^+ \to J/\psi K^+)$ and $A_{\mathrm{D}}(K^+)$ are considered as systematic uncertainties. They introduce correlations among the bins that are considered when the integrated results are calculated.

The Λ_b^0 production asymmetry is calculated, in each kinematic bin, assuming that the number of produced hadrons of any species in the i-th bin containing a b quark, $N_{i,b}$, is equal to the number of

Table 2
Values of signal yields, A_{P} and A_{D} obtained from global fits for the two neutral B-meson decays under study.

Parameter	$\sqrt{s} = 7$ TeV		$\sqrt{s} = 8$ TeV	
	$B^0 \to J/\psi\, K^{*0}$	$B_s^0 \to D_s^- \pi^+$	$B^0 \to J/\psi\, K^{*0}$	$B_s^0 \to D_s^- \pi^+$
N_{sig}	95122 ± 369	16932 ± 174	221973 ± 569	36726 ± 250
A_{P}	-0.0113 ± 0.0063	-0.0001 ± 0.0166	-0.0109 ± 0.0042	0.0081 ± 0.0111
A_{D}	-0.0098 ± 0.0046	-0.0143 ± 0.0086	-0.0056 ± 0.0030	-0.0103 ± 0.0058

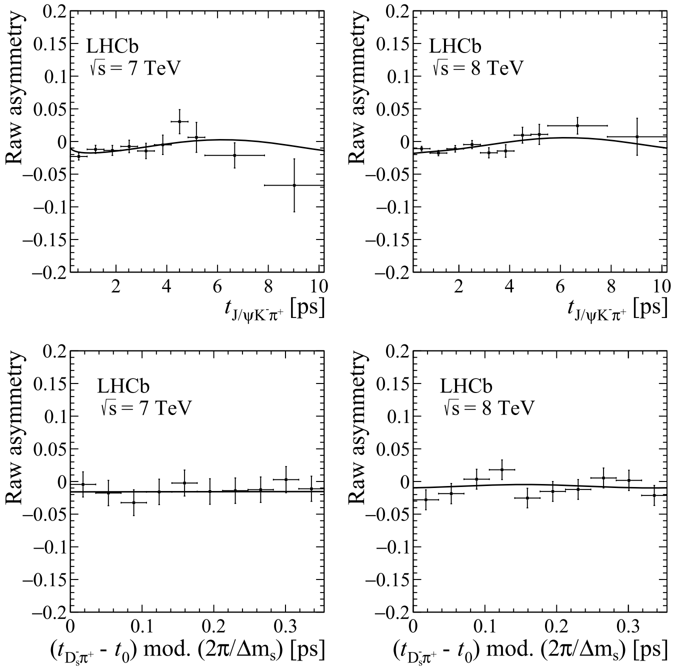

Fig. 4. Time-dependent raw asymmetries for candidates in the (top) $B^0 \to J/\psi\, K^{*0}$ and (bottom) $B_s^0 \to D_s^- \pi^+$ signal mass regions with the results of the global fits overlaid. Left and right plots correspond to data recorded in proton–proton collisions at centre-of-mass energies of 7 and 8 TeV, respectively. For the B_s^0 decay, the asymmetries are obtained by folding the decay-time distributions into one oscillation period, and the offset $t_0 = 0.2$ ps corresponds to the selection requirement on the decay time.

Table 3
Values of signal yields and raw asymmetries obtained from global fits in the case of the $B^+ \to J/\psi\, K^+$ decay.

Parameter	$\sqrt{s} = 7$ TeV	$\sqrt{s} = 8$ TeV
N_{sig}	265574 ± 576	619800 ± 908
A_{raw}	-0.017 ± 0.002	-0.014 ± 0.001

produced hadrons containing a $\overline{b}$ quark, $N_{i,\overline{b}}$, *i.e.* relying on Eq. (3). This assumption is strictly valid in the full phase space, but not necessarily in a specific bin. In the event that $N_{i,b} \neq N_{i,\overline{b}}$, $A_{\mathrm{P}}(\Lambda_b^0)$ is biased by the quantity

$$\delta z_i = \frac{N_{i,b} - N_{i,\overline{b}}}{N_{i,b} + N_{i,\overline{b}}} \cdot \frac{1}{f_{\Lambda_b^0}}.$$

Values for δz_i are studied using simulated events. Systematic uncertainties on $A_{\mathrm{P}}(\Lambda_b^0)$, in each kinematic bin, are assigned as half of the maximum variation from zero of the quantities $\delta z_i \pm \sigma(\delta z_i)$, where $\sigma(\delta z_i)$ is the related uncertainty.

The term $(f_c/f_{\Lambda_b^0}) \cdot A_{\mathrm{P}}(B_c^+)$, estimated to be $3 \cdot 10^{-5}$, can be safely neglected, while a systematic uncertainty related to neglecting the term $(f_{\mathrm{other}}/f_{\Lambda_b^0}) \cdot A_{\mathrm{P}}(\mathrm{other})$ has to be assessed. Amongst all other b baryons, the production rate of Ξ_b baryons is estimated from the simulation (which well reproduces the B^+, B^0, B_s^0 and Λ_b^0 fragmentation fractions) to be dominant, corresponding to about 1% of all b-hadron species produced in the primary collisions. On this basis, the neglected term can be evaluated as

$$\frac{f_{\mathrm{other}}}{f_{\Lambda_b^0}} A_{\mathrm{P}}(\mathrm{other}) \simeq \frac{f_{\Xi_b}}{f_{\Lambda_b^0}} A_{\mathrm{P}}(\Xi_b).$$

The value of $A_{\mathrm{P}}(\Xi_b)$ is found to be double that of $A_{\mathrm{P}}(\Lambda_b^0)$ in the simulation. A systematic uncertainty on $A_{\mathrm{P}}(\Lambda_b^0)$ is obtained by assuming $A_{\mathrm{P}}(\Xi_b) = 2\, A_{\mathrm{P}}(\Lambda_b^0)$.

The dominant systematic uncertainties for the B^+ and B^0 cases are related to the measured value of $A_{CP}(B^+ \to J/\psi\, K^+)$ and to $|q/p|_{B^0}$, respectively. The systematic uncertainty associated with the signal mass shape is the main source for the B_s^0 case, while it is the one related to neglecting the term $f_{\mathrm{other}}/f_{\Lambda_b^0} \cdot A_{\mathrm{P}}(\mathrm{other})$ in Eq. (3) in the case of the Λ_b^0 decay. All the systematic uncertainties are summed in quadrature for each kinematic bin. Their values are reported, together with the final measurements, in Tables 6–9 in the Appendix.

When the integrated results are calculated, all the systematic uncertainties estimated for each bin are propagated according to Eq. (4) and correlations among the bins are taken into account. An additional systematic uncertainty is considered by studying how the integrated values vary in the case that the values of ω_i are measured using a data driven approach. In this case ω_i^{data} is measured as

$$\omega_i^{\mathrm{data}} = \frac{N_i}{\varepsilon_i^{\mathrm{total}}} \Big/ \sum_i \frac{N_i}{\varepsilon_i^{\mathrm{total}}}$$

where $\varepsilon_i^{\mathrm{total}}$ is the total reconstruction efficiency, obtained as a combination of the selection efficiency, determined from simulation, and PID and trigger efficiencies, measured from data. Differences in the central values between A_{P} calculated using either ω_i or ω_i^{data} are found to be small for all the decay modes. Table 4 summarizes systematic uncertainties associated with the integrated measurements.

8. Results and conclusions

Using a data sample corresponding to an integrated luminosity of 3.0 fb^{-1}, the B^+, B^0 and B_s^0 hadron production asymmetries have been determined independently for each (p_{T}, y) bin and then combined using Eq. (3) to derive the Λ_b^0 production asymmetry. Tables 6–9, in the Appendix, report the final results.

The B^+, B^0, B_s^0 and Λ_b^0 hadron production asymmetries are also determined integrating over p_{T} or y, in the range $0 < p_{\mathrm{T}} < 30$ GeV/c and $2.1 < y < 4.5$ for B^+ and B^0 decays, and in the range $2 < p_{\mathrm{T}} < 30$ GeV/c and $2.1 < y < 4.5$ for B_s^0 and Λ_b^0 decay. The corresponding numerical values are reported in Tables 10–17, in the Appendix, and in Figs. 5–8, where the results of the fits with a constant and a first-order polynomial function are also shown. Table 5 reports the values of the fit parameters. No evidence for any dependence is observed. Finally, integrating over both p_{T} and y, the b-hadron production asymmetries are found to be

Table 4
Absolute values of systematic uncertainties for integrated production asymmetries. The total systematic uncertainties are obtained by summing the individual contributions in quadrature.

Source	Uncertainty [$\sqrt{s}$ = 7 TeV]			
	$A_{\rm P}(B^+)$	$A_{\rm P}(B^0)$	$A_{\rm P}(B_s^0)$	$A_{\rm P}(\Lambda_b^0)$
Signal mass shape	0.0016	0.0005	0.0036	0.0024
Decay-time bias	0.0000	0.0000	0.0008	0.0004
Δm_d, Δm_s	0.0000	0.0001	0.0014	0.0007
Decay-time resolution	0.0000	0.0000	0.0026	0.0014
Final-state radiation	0.0000	0.0001	0.0000	0.0001
Decay-time reconstruction efficiency	0.0000	0.0001	0.0000	0.0001
Combinatorial background mass shape	0.0003	0.0000	0.0004	0.0003
Partially reconstructed background mass shape	0.0000	0.0000	0.0029	0.0015
$\Delta\Gamma_s$	0.0000	0.0000	0.0000	0.0000
$A_{\rm D}(K^+)$	0.0018	0.0000	0.0000	0.0013
$\vert q/p\vert_{B^0}$, $\vert q/p\vert_{B_s^0}$	0.0000	0.0009	0.0021	0.0013
Uncertainties from fragmentation fractions	0.0000	0.0000	0.0000	0.0058
Difference between ω_i or $\omega_i^{\rm data}$	0.0003	0.0003	0.0003	0.0003
Neglecting term with $A_{\rm P}(\Xi_b)$ in Eq. (3)	0.0000	0.0000	0.0000	0.0071
Validity of $N_b = N_{\overline{b}}$ in each bin	0.0000	0.0000	0.0000	0.0032
$A_{CP}(B^+ \to J/\psi K^+)$	0.0028	0.0000	0.0000	0.0028
$A_{\rm D}(\overline{K}^0)$	0.0001	0.0000	0.0000	0.0002
Total systematic uncertainty	0.0037	0.0011	0.0059	0.0108

Source	Uncertainty [$\sqrt{s}$ = 8 TeV]			
	$A_{\rm P}(B^+)$	$A_{\rm P}(B^0)$	$A_{\rm P}(B_s^0)$	$A_{\rm P}(\Lambda_b^0)$
Signal mass shape	0.0006	0.0004	0.0035	0.0021
Decay-time bias	0.0000	0.0000	0.0008	0.0004
Δm_d, Δm_s	0.0000	0.0001	0.0015	0.0008
Decay-time resolution	0.0000	0.0000	0.0028	0.0016
Final-state radiation	0.0000	0.0001	0.0001	0.0001
Decay-time reconstruction efficiency	0.0000	0.0001	0.0001	0.0001
Combinatorial background mass shape	0.0002	0.0000	0.0004	0.0003
Partially reconstructed background mass shape	0.0000	0.0000	0.0027	0.0015
$\Delta\Gamma_s$	0.0000	0.0000	0.0001	0.0001
$A_{\rm D}(K^+)$	0.0014	0.0000	0.0000	0.0011
$\vert q/p\vert_{B^0}$, $\vert q/p\vert_{B_s^0}$	0.0000	0.0009	0.0021	0.0014
Uncertainties from fragmentation fractions	0.0000	0.0000	0.0000	0.0025
Difference between ω_i or $\omega_i^{\rm data}$	0.0002	0.0003	0.0003	0.0003
Neglecting term with $A_{\rm P}(\Xi_b)$ in Eq. (3)	0.0000	0.0000	0.0000	0.0046
Validity of $N_b = N_{\overline{b}}$ in each bin	0.0000	0.0000	0.0000	0.0033
$A_{CP}(B^+ \to J/\psi K^+)$	0.0028	0.0000	0.0000	0.0027
$A_{\rm D}(\overline{K}^0)$	0.0001	0.0000	0.0000	0.0002
Total systematic uncertainty	0.0032	0.0010	0.0059	0.0076

$$
\begin{aligned}
A_{\rm P}(B^+)_{\sqrt{s}=7\ {\rm TeV}} &= -0.0023 \pm 0.0024 \pm 0.0037,\\
A_{\rm P}(B^+)_{\sqrt{s}=8\ {\rm TeV}} &= -0.0074 \pm 0.0015 \pm 0.0032,\\
A_{\rm P}(B^0)_{\sqrt{s}=7\ {\rm TeV}} &= 0.0044 \pm 0.0088 \pm 0.0011,\\
A_{\rm P}(B^0)_{\sqrt{s}=8\ {\rm TeV}} &= -0.0140 \pm 0.0055 \pm 0.0010,\\
A_{\rm P}(B_s^0)_{\sqrt{s}=7\ {\rm TeV}} &= -0.0065 \pm 0.0288 \pm 0.0059,\\
A_{\rm P}(B_s^0)_{\sqrt{s}=8\ {\rm TeV}} &= 0.0198 \pm 0.0190 \pm 0.0059,\\
A_{\rm P}(\Lambda_b^0)_{\sqrt{s}=7\ {\rm TeV}} &= -0.0011 \pm 0.0253 \pm 0.0108,\\
A_{\rm P}(\Lambda_b^0)_{\sqrt{s}=8\ {\rm TeV}} &= 0.0344 \pm 0.0161 \pm 0.0076,
\end{aligned}
$$

where the first error is statistical and the second is systematic. All the results are consistent with zero within 2.5 standard deviations. The results of this analysis supersede the previous LHCb results of Ref. [6]. These measurements, once integrated using appropriate weights for any reconstructed B^+, B^0, B^0, Λ_b^0 decay in LHCb, can be used to determine effective production asymmetries, as inputs for *CP* violation measurements with the LHCb data.

Acknowledgements

We express our gratitude to our colleagues in the CERN accelerator departments for the excellent performance of the LHC. We thank the technical and administrative staff at the LHCb institutes. We acknowledge support from CERN and from the national agencies: CAPES, CNPq, FAPERJ and FINEP (Brazil); MOST and NSFC (China); CNRS/IN2P3 (France); BMBF, DFG and MPG (Germany); INFN (Italy); NWO (The Netherlands); MNiSW and NCN (Poland); MEN/IFA (Romania); MinES and FASO (Russia); MINECO (Spain); SNSF and SER (Switzerland); NASU (Ukraine); STFC (United Kingdom); NSF (USA). We acknowledge the computing resources that are provided by CERN, IN2P3 (France), KIT and DESY (Germany), INFN (Italy), SURF (The Netherlands), PIC (Spain), GridPP (United Kingdom), RRCKI and Yandex LLC (Russia), CSCS (Switzerland), IFIN-HH (Romania), CBPF (Brazil), PL-GRID (Poland) and OSC (USA). We are indebted to the communities behind the multiple open source software packages on which we depend. Individual groups or members have received support from AvH Foundation (Germany), EPLANET, Marie Skłodowska-Curie Actions and ERC (European Union), Conseil Général de Haute-Savoie, Labex ENIGMASS and OCEVU, Région Auvergne (France), RFBR and Yandex LLC (Russia), GVA, XuntaGal and GENCAT (Spain), Herchel Smith Fund, The Royal Society, Royal Commission for the Exhibition of 1851 and the Leverhulme Trust (United Kingdom).

Table 5
Values for m and q and their correlation coefficient (ρ) obtained from fits to the values reported in Tables 10–17 with a first order polynomial function (FOPF), $A_{\mathrm{P}}(b\,\text{hadron}) = ax + b$ with $x = p_{\mathrm{T}}, y$. The label SL indicates the fit to the values with a straight line.

$\sqrt{s} = 7$ TeV				
p_{T}	B^+	B^0	B^0_s	Λ^0_b
$a[c/\mathrm{GeV} \cdot 10^{-4}]$	-3 ± 6	7 ± 14	-33 ± 26	10 ± 60
$b[10^{-3}]$	-1 ± 5	-3 ± 12	44 ± 37	7 ± 50
$\rho(m,q)$	-0.59	-0.78	-0.89	-0.85
fit χ^2/ndf (SL)	1.05	1.67	1.67	2.03
fit χ^2/ndf (FOPF)	0.95	1.50	1.68	1.34

$\sqrt{s} = 8$ TeV				
p_{T}	B^+	B^0	B^0_s	Λ^0_b
$a[c/\mathrm{GeV} \cdot 10^{-4}]$	-5 ± 4	12 ± 9	2 ± 18	30 ± 30
$b[10^{-3}]$	-5 ± 4	-18 ± 8	8 ± 25	12 ± 32
$\rho(m,q)$	-0.49	-0.78	-0.89	-0.84
fit χ^2/ndf (SL)	0.99	0.54	1.80	0.07
fit χ^2/ndf (FOPF)	1.12	0.67	1.19	0.28

$\sqrt{s} = 7$ TeV				
y	B^+	B^0	B^0_s	Λ^0_b
$a[10^{-4}]$	22 ± 45	-71 ± 141	-542 ± 469	810 ± 420
$b[10^{-3}]$	-12 ± 14	-12 ± 46	165 ± 153	-240 ± 130
$\rho(m,q)$	-0.96	-0.99	-0.99	-0.98
fit χ^2/ndf (SL)	1.36	2.79	0.48	0.86
fit χ^2/ndf (FOPF)	1.17	2.36	0.91	2.29

$\sqrt{s} = 8$ TeV				
y	B^+	B^0	B^0_s	Λ^0_b
$a[10^{-4}]$	-86 ± 29	-44 ± 100	-217 ± 321	470 ± 280
$b[10^{-3}]$	19 ± 9	-4 ± 32	85 ± 105	-111 ± 90
$\rho(m,q)$	-0.93	-0.99	-0.98	-0.98
fit χ^2/ndf (SL)	1.10	0.86	0.42	1.35
fit χ^2/ndf (FOPF)	2.43	0.75	0.44	2.23

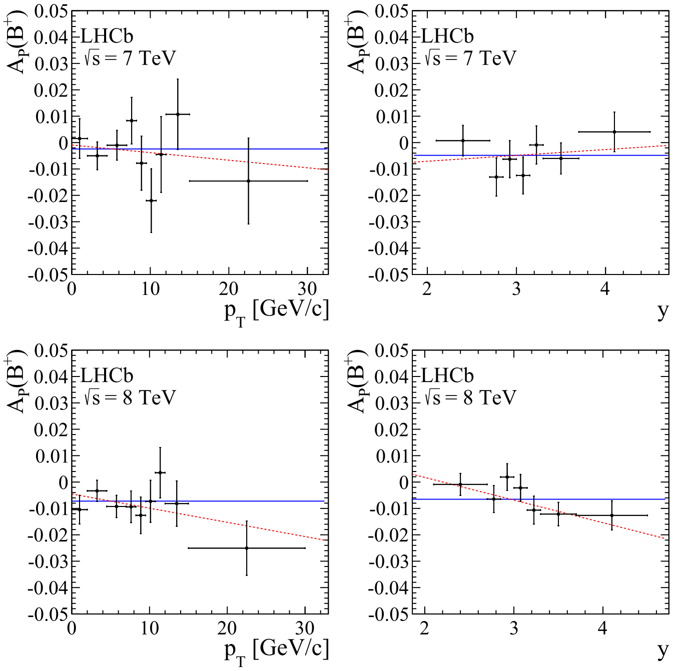

Fig. 5. Dependence of $A_{\mathrm{P}}(B^+)$, for data collected in proton–proton collisions with centre-of-mass of energies of (top) 7 and (bottom) 8 TeV, on (left) p_{T} and (right) y. The results of fits using a straight line with zero (solid line) or floating slope parameter (dashed line) are also shown. The fits take into account the correlations amongst the bins.

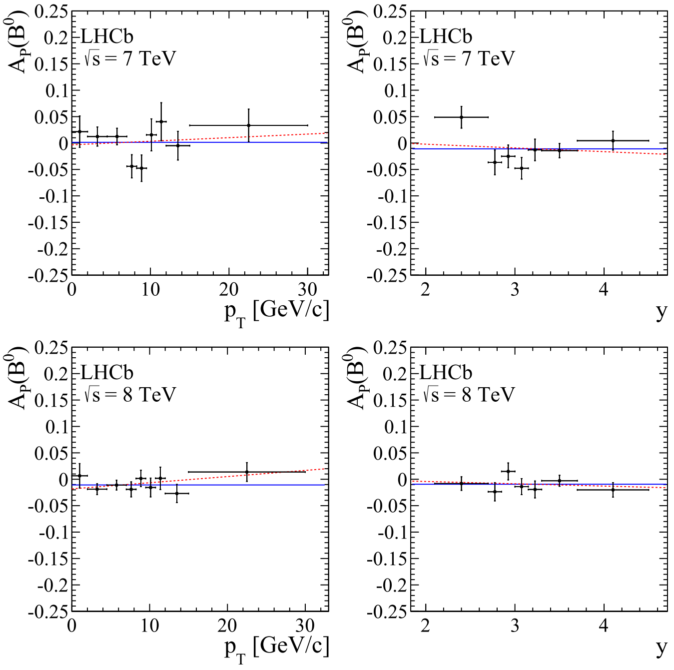

Fig. 6. Dependence of $A_{\mathrm{P}}(B^0)$, for data collected in proton–proton collisions with centre-of-mass of energies of (top) 7 and (bottom) 8 TeV, on (left) p_{T} and (right) y. The results of fits using a straight line with zero (solid line) or floating slope parameter (dashed line) are also shown. The fits take into account the correlations amongst the bins.

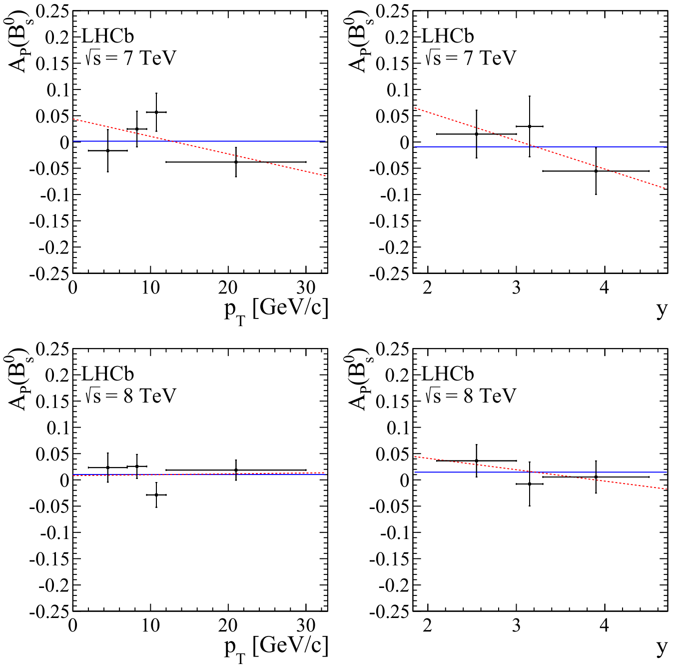

Fig. 7. Dependence of $A_{\mathrm{P}}(B_s^0)$, for data collected in proton–proton collisions with centre-of-mass of energies of (top) 7 and (bottom) 8 TeV, on (left) p_{T} and (right) y. The results of fits with a straight line with zero (solid line) or floating slope parameter (dashed line) are also shown. The fits take into account the correlations amongst the bins.

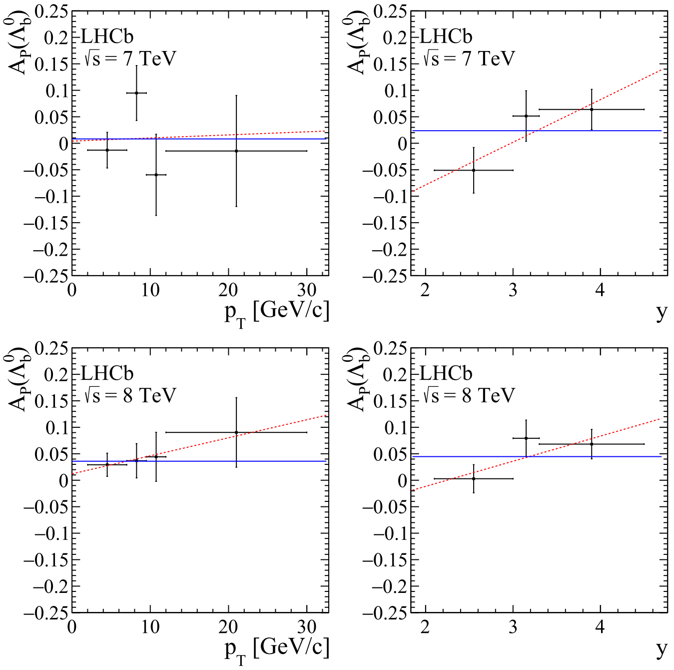

Fig. 8. Dependence of $A_{\mathrm{P}}(\Lambda_b^0)$, for data collected in proton–proton collisions with centre-of-mass of energies of (top) 7 and (bottom) 8 TeV, on (left) p_{T} and (right) y. The results of fits with a straight line with zero (solid line) or floating slope parameter (dashed line) are also shown. The fits take into account the correlations amongst the bins.

Appendix

Table 6
Values of $A_{\mathrm{P}}(B^+)$ and $A_{\mathrm{P}}(B^0)$ in each kinematic bin for data collected in proton–proton collisions at centre-of-mass energy of 7 TeV. The first uncertainties are statistical and the second systematic.

p_{T} [GeV/c]	y	$A_{\mathrm{P}}(B^+)_{\sqrt{s}=7\ \mathrm{TeV}}$	$A_{\mathrm{P}}(B^0)_{\sqrt{s}=7\ \mathrm{TeV}}$
(0.00, 2.00)	(2.10, 2.70)	$0.0085 \pm 0.0156 \pm 0.0036$	$0.0722 \pm 0.0770 \pm 0.0010$
(0.00, 2.00)	(2.70, 2.85)	$-0.0014 \pm 0.0191 \pm 0.0036$	$-0.1108 \pm 0.0815 \pm 0.0020$
(0.00, 2.00)	(2.85, 3.00)	$0.0016 \pm 0.0177 \pm 0.0036$	$-0.0300 \pm 0.0733 \pm 0.0024$
(0.00, 2.00)	(3.00, 3.15)	$-0.0052 \pm 0.0171 \pm 0.0036$	$-0.0849 \pm 0.0624 \pm 0.0038$
(0.00, 2.00)	(3.15, 3.30)	$-0.0006 \pm 0.0171 \pm 0.0037$	$-0.0662 \pm 0.0638 \pm 0.0035$
(0.00, 2.00)	(3.30, 3.70)	$0.0107 \pm 0.0110 \pm 0.0040$	$0.0116 \pm 0.0397 \pm 0.0011$
(0.00, 2.00)	(3.70, 4.50)	$-0.0104 \pm 0.0141 \pm 0.0046$	$0.0702 \pm 0.0462 \pm 0.0013$
(2.00, 4.50)	(2.10, 2.70)	$0.0007 \pm 0.0088 \pm 0.0036$	$0.0691 \pm 0.0392 \pm 0.0017$
(2.00, 4.50)	(2.70, 2.85)	$-0.0171 \pm 0.0112 \pm 0.0036$	$0.0136 \pm 0.0409 \pm 0.0013$
(2.00, 4.50)	(2.85, 3.00)	$-0.0120 \pm 0.0105 \pm 0.0036$	$-0.0284 \pm 0.0375 \pm 0.0010$
(2.00, 4.50)	(3.00, 3.15)	$-0.0269 \pm 0.0101 \pm 0.0037$	$-0.0273 \pm 0.0360 \pm 0.0009$
(2.00, 4.50)	(3.15, 3.30)	$0.0043 \pm 0.0102 \pm 0.0038$	$0.0137 \pm 0.0351 \pm 0.0015$
(2.00, 4.50)	(3.30, 3.70)	$-0.0167 \pm 0.0071 \pm 0.0041$	$-0.0273 \pm 0.0230 \pm 0.0028$
(2.00, 4.50)	(3.70, 4.50)	$0.0053 \pm 0.0098 \pm 0.0045$	$-0.0269 \pm 0.0279 \pm 0.0013$
(4.50, 7.00)	(2.10, 2.70)	$0.0023 \pm 0.0087 \pm 0.0035$	$0.0597 \pm 0.0329 \pm 0.0039$
(4.50, 7.00)	(2.70, 2.85)	$-0.0002 \pm 0.0120 \pm 0.0037$	$-0.0177 \pm 0.0404 \pm 0.0010$
(4.50, 7.00)	(2.85, 3.00)	$0.0034 \pm 0.0116 \pm 0.0038$	$-0.0103 \pm 0.0362 \pm 0.0019$
(4.50, 7.00)	(3.00, 3.15)	$0.0092 \pm 0.0115 \pm 0.0039$	$-0.0696 \pm 0.0372 \pm 0.0016$
(4.50, 7.00)	(3.15, 3.30)	$-0.0092 \pm 0.0120 \pm 0.0042$	$-0.0444 \pm 0.0359 \pm 0.0015$
(4.50, 7.00)	(3.30, 3.70)	$-0.0168 \pm 0.0088 \pm 0.0044$	$-0.0214 \pm 0.0234 \pm 0.0010$
(4.50, 7.00)	(3.70, 4.50)	$0.0010 \pm 0.0129 \pm 0.0044$	$0.0192 \pm 0.0316 \pm 0.0013$
(7.00, 8.25)	(2.10, 2.70)	$0.0031 \pm 0.0140 \pm 0.0036$	$-0.0239 \pm 0.0441 \pm 0.0025$
(7.00, 8.25)	(2.70, 2.85)	$-0.0591 \pm 0.0208 \pm 0.0039$	$-0.2197 \pm 0.0602 \pm 0.0017$
(7.00, 8.25)	(2.85, 3.00)	$-0.0089 \pm 0.0203 \pm 0.0040$	$-0.0619 \pm 0.0595 \pm 0.0031$
(7.00, 8.25)	(3.00, 3.15)	$0.0016 \pm 0.0213 \pm 0.0043$	$-0.0151 \pm 0.0590 \pm 0.0047$
(7.00, 8.25)	(3.15, 3.30)	$-0.0205 \pm 0.0222 \pm 0.0044$	$-0.0037 \pm 0.0566 \pm 0.0039$
(7.00, 8.25)	(3.30, 3.70)	$0.0303 \pm 0.0172 \pm 0.0046$	$-0.0305 \pm 0.0406 \pm 0.0018$

(*continued on next page*)

Table 6 (*continued*)

p_{T} [GeV/c]	y	$A_{\mathrm{P}}(B^{+})_{\sqrt{s}=7\ \mathrm{TeV}}$	$A_{\mathrm{P}}(B^{0})_{\sqrt{s}=7\ \mathrm{TeV}}$
(7.00, 8.25)	(3.70, 4.50)	$0.0603 \pm 0.0259 \pm 0.0047$	$-0.0348 \pm 0.0516 \pm 0.0018$
(8.25, 9.50)	(2.10, 2.70)	$-0.0134 \pm 0.0157 \pm 0.0037$	$-0.0442 \pm 0.0477 \pm 0.0087$
(8.25, 9.50)	(2.70, 2.85)	$-0.0099 \pm 0.0246 \pm 0.0039$	$-0.0506 \pm 0.0652 \pm 0.0028$
(8.25, 9.50)	(2.85, 3.00)	$-0.0112 \pm 0.0246 \pm 0.0042$	$-0.0611 \pm 0.0674 \pm 0.0043$
(8.25, 9.50)	(3.00, 3.15)	$-0.0613 \pm 0.0251 \pm 0.0044$	$-0.0015 \pm 0.0695 \pm 0.0024$
(8.25, 9.50)	(3.15, 3.30)	$0.0552 \pm 0.0279 \pm 0.0045$	$0.0219 \pm 0.0731 \pm 0.0014$
(8.25, 9.50)	(3.30, 3.70)	$-0.0038 \pm 0.0216 \pm 0.0046$	$-0.0621 \pm 0.0478 \pm 0.0032$
(8.25, 9.50)	(3.70, 4.50)	$0.0047 \pm 0.0342 \pm 0.0047$	$-0.0856 \pm 0.0637 \pm 0.0025$
(9.50, 10.75)	(2.10, 2.70)	$-0.0249 \pm 0.0182 \pm 0.0037$	$0.0408 \pm 0.0525 \pm 0.0089$
(9.50, 10.75)	(2.70, 2.85)	$-0.0113 \pm 0.0292 \pm 0.0041$	$0.0228 \pm 0.0759 \pm 0.0036$
(9.50, 10.75)	(2.85, 3.00)	$-0.0241 \pm 0.0290 \pm 0.0045$	$0.0102 \pm 0.0904 \pm 0.0017$
(9.50, 10.75)	(3.00, 3.15)	$0.0267 \pm 0.0318 \pm 0.0045$	$-0.0586 \pm 0.0847 \pm 0.0023$
(9.50, 10.75)	(3.15, 3.30)	$0.0118 \pm 0.0352 \pm 0.0048$	$-0.0577 \pm 0.0775 \pm 0.0012$
(9.50, 10.75)	(3.30, 3.70)	$-0.0164 \pm 0.0281 \pm 0.0048$	$0.0624 \pm 0.0577 \pm 0.0016$
(9.50, 10.75)	(3.70, 4.50)	$-0.0605 \pm 0.0411 \pm 0.0049$	$-0.0328 \pm 0.0946 \pm 0.0021$
(10.75, 12.00)	(2.10, 2.70)	$-0.0200 \pm 0.0206 \pm 0.0038$	$0.0154 \pm 0.0636 \pm 0.0023$
(10.75, 12.00)	(2.70, 2.85)	$-0.0068 \pm 0.0344 \pm 0.0044$	$-0.0104 \pm 0.1017 \pm 0.0044$
(10.75, 12.00)	(2.85, 3.00)	$-0.0017 \pm 0.0362 \pm 0.0045$	$0.0179 \pm 0.0849 \pm 0.0040$
(10.75, 12.00)	(3.15, 3.30)	$-0.0239 \pm 0.0441 \pm 0.0047$	$0.0478 \pm 0.0835 \pm 0.0025$
(10.75, 12.00)	(3.00, 3.15)	$-0.0181 \pm 0.0411 \pm 0.0047$	$0.1481 \pm 0.0890 \pm 0.0024$
(10.75, 12.00)	(3.30, 3.70)	$0.0058 \pm 0.0362 \pm 0.0048$	$0.0377 \pm 0.0731 \pm 0.0037$
(10.75, 12.00)	(3.70, 4.50)	$0.0485 \pm 0.0547 \pm 0.0051$	$0.1058 \pm 0.1181 \pm 0.0018$
(12.00, 15.00)	(2.10, 2.70)	$0.0059 \pm 0.0174 \pm 0.0039$	$-0.0071 \pm 0.0446 \pm 0.0039$
(12.00, 15.00)	(2.70, 2.85)	$0.0210 \pm 0.0321 \pm 0.0046$	$0.0264 \pm 0.0924 \pm 0.0042$
(12.00, 15.00)	(2.85, 3.00)	$0.0092 \pm 0.0334 \pm 0.0062$	$0.0230 \pm 0.0775 \pm 0.0046$
(12.00, 15.00)	(3.00, 3.15)	$-0.0267 \pm 0.0386 \pm 0.0050$	$-0.1190 \pm 0.0791 \pm 0.0040$
(12.00, 15.00)	(3.15, 3.30)	$-0.0516 \pm 0.0420 \pm 0.0046$	$0.1330 \pm 0.0909 \pm 0.0029$
(12.00, 15.00)	(3.30, 3.70)	$0.0071 \pm 0.0349 \pm 0.0052$	$0.0469 \pm 0.0588 \pm 0.0021$
(12.00, 15.00)	(3.70, 4.50)	$0.0748 \pm 0.0542 \pm 0.0049$	$-0.1026 \pm 0.0854 \pm 0.0031$
(15.00, 30.00)	(2.10, 2.70)	$0.0116 \pm 0.0188 \pm 0.0040$	$0.0703 \pm 0.0456 \pm 0.0014$
(15.00, 30.00)	(2.70, 2.85)	$-0.0763 \pm 0.0401 \pm 0.0046$	$-0.0009 \pm 0.0748 \pm 0.0034$
(15.00, 30.00)	(2.85, 3.00)	$-0.0541 \pm 0.0458 \pm 0.0047$	$-0.0550 \pm 0.0755 \pm 0.0049$
(15.00, 30.00)	(3.00, 3.15)	$-0.0449 \pm 0.0512 \pm 0.0046$	$-0.1637 \pm 0.0925 \pm 0.0026$
(15.00, 30.00)	(3.15, 3.30)	$0.0011 \pm 0.0599 \pm 0.0073$	$0.0456 \pm 0.1119 \pm 0.0018$
(15.00, 30.00)	(3.30, 3.70)	$0.0089 \pm 0.0502 \pm 0.0048$	$-0.0193 \pm 0.0777 \pm 0.0027$
(15.00, 30.00)	(3.70, 4.50)	$-0.0662 \pm 0.0827 \pm 0.0186$	$0.1690 \pm 0.1332 \pm 0.0030$

Table 7

Values of $A_{\mathrm{P}}(B^{+})$ and $A_{\mathrm{P}}(B^{0})$ in each kinematic bin for data collected in proton–proton collisions at centre-of-mass energy of 8 TeV. The first uncertainties are statistical and the second systematic.

p_{T} [GeV/c]	y	$A_{\mathrm{P}}(B^{+})_{\sqrt{s}=8\ \mathrm{TeV}}$	$A_{\mathrm{P}}(B^{0})_{\sqrt{s}=8\ \mathrm{TeV}}$
(0.00, 2.00)	(2.10, 2.70)	$-0.0178 \pm 0.0097 \pm 0.0031$	$0.0068 \pm 0.0537 \pm 0.0009$
(0.00, 2.00)	(2.70, 2.85)	$-0.0027 \pm 0.0126 \pm 0.0031$	$-0.0735 \pm 0.0719 \pm 0.0017$
(0.00, 2.00)	(2.85, 3.00)	$0.0093 \pm 0.0120 \pm 0.0031$	$0.0503 \pm 0.0628 \pm 0.0011$
(0.00, 2.00)	(3.00, 3.15)	$0.0005 \pm 0.0119 \pm 0.0031$	$0.0086 \pm 0.0549 \pm 0.0034$
(0.00, 2.00)	(3.15, 3.30)	$-0.0230 \pm 0.0119 \pm 0.0033$	$0.0817 \pm 0.0617 \pm 0.0016$
(0.00, 2.00)	(3.30, 3.70)	$-0.0120 \pm 0.0080 \pm 0.0033$	$0.0668 \pm 0.0367 \pm 0.0009$
(0.00, 2.00)	(3.70, 4.50)	$-0.0077 \pm 0.0103 \pm 0.0037$	$-0.0419 \pm 0.0453 \pm 0.0010$
(2.00, 4.50)	(2.10, 2.70)	$0.0050 \pm 0.0054 \pm 0.0031$	$-0.0192 \pm 0.0234 \pm 0.0013$
(2.00, 4.50)	(2.70, 2.85)	$-0.0076 \pm 0.0073 \pm 0.0031$	$-0.0070 \pm 0.0291 \pm 0.0009$
(2.00, 4.50)	(2.85, 3.00)	$0.0009 \pm 0.0070 \pm 0.0031$	$-0.0088 \pm 0.0278 \pm 0.0009$
(2.00, 4.50)	(3.00, 3.15)	$-0.0046 \pm 0.0069 \pm 0.0032$	$-0.0213 \pm 0.0271 \pm 0.0009$
(2.00, 4.50)	(3.15, 3.30)	$-0.0018 \pm 0.0070 \pm 0.0032$	$-0.0635 \pm 0.0260 \pm 0.0012$
(2.00, 4.50)	(3.30, 3.70)	$-0.0081 \pm 0.0049 \pm 0.0034$	$-0.0169 \pm 0.0174 \pm 0.0009$
(2.00, 4.50)	(3.70, 4.50)	$-0.0133 \pm 0.0067 \pm 0.0036$	$-0.0131 \pm 0.0203 \pm 0.0009$
(4.50, 7.00)	(2.10, 2.70)	$-0.0045 \pm 0.0054 \pm 0.0031$	$-0.0074 \pm 0.0192 \pm 0.0028$
(4.50, 7.00)	(2.70, 2.85)	$-0.0002 \pm 0.0077 \pm 0.0031$	$-0.0440 \pm 0.0264 \pm 0.0027$
(4.50, 7.00)	(2.85, 3.00)	$-0.0019 \pm 0.0075 \pm 0.0032$	$0.0315 \pm 0.0235 \pm 0.0028$
(4.50, 7.00)	(3.00, 3.15)	$-0.0107 \pm 0.0076 \pm 0.0033$	$-0.0203 \pm 0.0233 \pm 0.0020$
(4.50, 7.00)	(3.15, 3.30)	$-0.0175 \pm 0.0078 \pm 0.0034$	$-0.0248 \pm 0.0234 \pm 0.0010$
(4.50, 7.00)	(3.30, 3.70)	$-0.0241 \pm 0.0059 \pm 0.0035$	$-0.0254 \pm 0.0159 \pm 0.0010$
(4.50, 7.00)	(3.70, 4.50)	$-0.0101 \pm 0.0087 \pm 0.0036$	$-0.0015 \pm 0.0213 \pm 0.0010$

Table 7 (*continued*)

p_T [GeV/c]	y	$A_P(B^+)_{\sqrt{s}=8\text{ TeV}}$	$A_P(B^0)_{\sqrt{s}=8\text{ TeV}}$
(7.00, 8.25)	(2.10, 2.70)	$-0.0052 \pm 0.0086 \pm 0.0031$	$0.0080 \pm 0.0276 \pm 0.0028$
(7.00, 8.25)	(2.70, 2.85)	$-0.0177 \pm 0.0131 \pm 0.0033$	$-0.0383 \pm 0.0390 \pm 0.0014$
(7.00, 8.25)	(2.85, 3.00)	$-0.0083 \pm 0.0132 \pm 0.0033$	$-0.0543 \pm 0.0382 \pm 0.0025$
(7.00, 8.25)	(3.00, 3.15)	$0.0065 \pm 0.0134 \pm 0.0035$	$-0.0575 \pm 0.0377 \pm 0.0012$
(7.00, 8.25)	(3.15, 3.30)	$-0.0055 \pm 0.0144 \pm 0.0040$	$-0.0120 \pm 0.0379 \pm 0.0013$
(7.00, 8.25)	(3.30, 3.70)	$-0.0003 \pm 0.0111 \pm 0.0036$	$-0.0089 \pm 0.0268 \pm 0.0044$
(7.00, 8.25)	(3.70, 4.50)	$-0.0300 \pm 0.0168 \pm 0.0036$	$-0.0486 \pm 0.0364 \pm 0.0022$
(8.25, 9.50)	(2.10, 2.70)	$-0.0038 \pm 0.0097 \pm 0.0031$	$-0.0215 \pm 0.0286 \pm 0.0017$
(8.25, 9.50)	(2.70, 2.85)	$-0.0070 \pm 0.0153 \pm 0.0033$	$0.0710 \pm 0.0415 \pm 0.0013$
(8.25, 9.50)	(2.85, 3.00)	$-0.0228 \pm 0.0157 \pm 0.0034$	$0.0123 \pm 0.0395 \pm 0.0010$
(8.25, 9.50)	(3.00, 3.15)	$-0.0236 \pm 0.0164 \pm 0.0037$	$0.0747 \pm 0.0411 \pm 0.0023$
(8.25, 9.50)	(3.15, 3.30)	$-0.0252 \pm 0.0182 \pm 0.0042$	$-0.0533 \pm 0.0459 \pm 0.0025$
(8.25, 9.50)	(3.30, 3.70)	$-0.0036 \pm 0.0141 \pm 0.0037$	$0.0152 \pm 0.0299 \pm 0.0009$
(8.25, 9.50)	(3.70, 4.50)	$-0.0293 \pm 0.0220 \pm 0.0037$	$-0.0063 \pm 0.0448 \pm 0.0034$
(9.50, 10.75)	(2.10, 2.70)	$0.0060 \pm 0.0109 \pm 0.0032$	$0.0022 \pm 0.0324 \pm 0.0022$
(9.50, 10.75)	(2.70, 2.85)	$-0.0011 \pm 0.0183 \pm 0.0036$	$0.0429 \pm 0.0491 \pm 0.0050$
(9.50, 10.75)	(2.85, 3.00)	$0.0122 \pm 0.0182 \pm 0.0036$	$0.0513 \pm 0.0509 \pm 0.0021$
(9.50, 10.75)	(3.00, 3.15)	$0.0067 \pm 0.0204 \pm 0.0037$	$-0.0898 \pm 0.0499 \pm 0.0059$
(9.50, 10.75)	(3.15, 3.30)	$-0.0462 \pm 0.0233 \pm 0.0037$	$-0.0220 \pm 0.0494 \pm 0.0034$
(9.50, 10.75)	(3.30, 3.70)	$-0.0290 \pm 0.0181 \pm 0.0037$	$-0.0204 \pm 0.0353 \pm 0.0013$
(9.50, 10.75)	(3.70, 4.50)	$-0.0243 \pm 0.0273 \pm 0.0037$	$-0.0849 \pm 0.0509 \pm 0.0026$
(10.75, 12.00)	(2.10, 2.70)	$0.0191 \pm 0.0128 \pm 0.0032$	$0.0034 \pm 0.0355 \pm 0.0056$
(10.75, 12.00)	(2.70, 2.85)	$-0.0562 \pm 0.0220 \pm 0.0034$	$-0.0193 \pm 0.0593 \pm 0.0026$
(10.75, 12.00)	(2.85, 3.00)	$0.0172 \pm 0.0233 \pm 0.0037$	$0.0198 \pm 0.0628 \pm 0.0066$
(10.75, 12.00)	(3.00, 3.15)	$-0.0080 \pm 0.0262 \pm 0.0044$	$-0.0056 \pm 0.0565 \pm 0.0012$
(10.75, 12.00)	(3.15, 3.30)	$0.0162 \pm 0.0282 \pm 0.0038$	$-0.0638 \pm 0.0582 \pm 0.0040$
(10.75, 12.00)	(3.30, 3.70)	$-0.0393 \pm 0.0233 \pm 0.0037$	$0.0205 \pm 0.0454 \pm 0.0083$
(10.75, 12.00)	(3.70, 4.50)	$0.0317 \pm 0.0353 \pm 0.0038$	$0.0139 \pm 0.0709 \pm 0.0009$
(12.00, 15.00)	(2.10, 2.70)	$0.0067 \pm 0.0106 \pm 0.0032$	$-0.0364 \pm 0.0278 \pm 0.0010$
(12.00, 15.00)	(2.70, 2.85)	$-0.0232 \pm 0.0195 \pm 0.0035$	$-0.0007 \pm 0.0525 \pm 0.0026$
(12.00, 15.00)	(2.85, 3.00)	$0.0171 \pm 0.0211 \pm 0.0047$	$0.0255 \pm 0.0467 \pm 0.0010$
(12.00, 15.00)	(3.00, 3.15)	$0.0065 \pm 0.0241 \pm 0.0046$	$0.0080 \pm 0.0521 \pm 0.0017$
(12.00, 15.00)	(3.15, 3.30)	$-0.0101 \pm 0.0273 \pm 0.0038$	$-0.0019 \pm 0.0491 \pm 0.0021$
(12.00, 15.00)	(3.30, 3.70)	$-0.0214 \pm 0.0219 \pm 0.0039$	$-0.0526 \pm 0.0373 \pm 0.0045$
(12.00, 15.00)	(3.70, 4.50)	$-0.0511 \pm 0.0340 \pm 0.0038$	$-0.0494 \pm 0.0605 \pm 0.0027$
(15.00, 30.00)	(2.10, 2.70)	$-0.0203 \pm 0.0115 \pm 0.0033$	$0.0217 \pm 0.0267 \pm 0.0012$
(15.00, 30.00)	(2.70, 2.85)	$-0.0340 \pm 0.0252 \pm 0.0036$	$-0.0204 \pm 0.0491 \pm 0.0038$
(15.00, 30.00)	(2.85, 3.00)	$-0.0231 \pm 0.0277 \pm 0.0055$	$0.0878 \pm 0.0520 \pm 0.0020$
(15.00, 30.00)	(3.00, 3.15)	$0.0347 \pm 0.0317 \pm 0.0037$	$0.0120 \pm 0.0534 \pm 0.0016$
(15.00, 30.00)	(3.15, 3.30)	$-0.0064 \pm 0.0379 \pm 0.0068$	$0.0153 \pm 0.0626 \pm 0.0025$
(15.00, 30.00)	(3.30, 3.70)	$-0.0221 \pm 0.0311 \pm 0.0042$	$-0.0647 \pm 0.0434 \pm 0.0013$
(15.00, 30.00)	(3.70, 4.50)	$-0.0987 \pm 0.0496 \pm 0.0063$	$0.0394 \pm 0.0777 \pm 0.0042$

Table 8
Values of $A_P(B_s^0)$ and $A_P(\Lambda_b^0)$ in each kinematic bin for data collected in proton–proton collisions at centre-of-mass energy of 7 TeV. The first uncertainties are statistical and the second systematic.

p_T [GeV/c]	y	$A_P(B_s^0)_{\sqrt{s}=7\text{ TeV}}$	$A_P(\Lambda_b^0)_{\sqrt{s}=7\text{ TeV}}$
(2.00, 7.00)	(2.10, 3.00)	$0.0166 \pm 0.0632 \pm 0.0125$	$-0.0892 \pm 0.0508 \pm 0.0214$
(2.00, 7.00)	(3.00, 3.30)	$0.0311 \pm 0.0773 \pm 0.0151$	$0.0507 \pm 0.0539 \pm 0.0208$
(2.00, 7.00)	(3.30, 4.50)	$-0.0833 \pm 0.0558 \pm 0.0132$	$0.0849 \pm 0.0401 \pm 0.0188$
(7.00, 9.50)	(2.10, 3.00)	$0.0364 \pm 0.0479 \pm 0.0068$	$0.1374 \pm 0.0697 \pm 0.0313$
(7.00, 9.50)	(3.00, 3.30)	$0.0206 \pm 0.0682 \pm 0.0127$	$0.0138 \pm 0.0913 \pm 0.0298$
(7.00, 9.50)	(3.30, 4.50)	$0.0058 \pm 0.0584 \pm 0.0089$	$0.0466 \pm 0.0770 \pm 0.0347$
(9.50, 12.00)	(2.10, 3.00)	$-0.0039 \pm 0.0456 \pm 0.0121$	$-0.0128 \pm 0.0985 \pm 0.0367$
(9.50, 12.00)	(3.00, 3.30)	$0.1095 \pm 0.0723 \pm 0.0179$	$-0.0848 \pm 0.1379 \pm 0.0452$
(9.50, 12.00)	(3.30, 4.50)	$0.1539 \pm 0.0722 \pm 0.0212$	$-0.1523 \pm 0.1414 \pm 0.0488$
(12.00, 30.00)	(2.10, 3.00)	$-0.0271 \pm 0.0336 \pm 0.0061$	$-0.0720 \pm 0.1248 \pm 0.0465$
(12.00, 30.00)	(3.00, 3.30)	$-0.0542 \pm 0.0612 \pm 0.0106$	$0.3291 \pm 0.2299 \pm 0.0918$
(12.00, 30.00)	(3.30, 4.50)	$-0.0586 \pm 0.0648 \pm 0.0150$	$-0.0571 \pm 0.2162 \pm 0.0800$

Table 9
Values of $A_{\mathrm{P}}(B_s^0)$ and $A_{\mathrm{P}}(\Lambda_b^0)$ in each kinematic bin for data collected in proton–proton collisions at centre-of-mass energy of 8 TeV. The first uncertainties are statistical and the second systematic.

p_{T} [GeV/c]	y	$A_{\mathrm{P}}(B_s^0)_{\sqrt{s}=8\ \mathrm{TeV}}$	$A_{\mathrm{P}}(\Lambda_b^0)_{\sqrt{s}=8\ \mathrm{TeV}}$
(2.00, 7.00)	(2.10, 3.00)	$0.0412 \pm 0.0416 \pm 0.0150$	$0.0032 \pm 0.0318 \pm 0.0139$
(2.00, 7.00)	(3.00, 3.30)	$-0.0241 \pm 0.0574 \pm 0.0079$	$0.0929 \pm 0.0392 \pm 0.0171$
(2.00, 7.00)	(3.30, 4.50)	$0.0166 \pm 0.0391 \pm 0.0092$	$0.0437 \pm 0.0284 \pm 0.0173$
(7.00, 9.50)	(2.10, 3.00)	$0.0482 \pm 0.0320 \pm 0.0067$	$0.0069 \pm 0.0434 \pm 0.0169$
(7.00, 9.50)	(3.00, 3.30)	$0.0983 \pm 0.0470 \pm 0.0155$	$0.0076 \pm 0.0589 \pm 0.0259$
(7.00, 9.50)	(3.30, 4.50)	$-0.0430 \pm 0.0386 \pm 0.0079$	$0.1053 \pm 0.0524 \pm 0.0252$
(9.50, 12.00)	(2.10, 3.00)	$0.0067 \pm 0.0303 \pm 0.0063$	$-0.0512 \pm 0.0594 \pm 0.0215$
(9.50, 12.00)	(3.00, 3.30)	$-0.1283 \pm 0.0503 \pm 0.0171$	$0.2355 \pm 0.0877 \pm 0.0399$
(9.50, 12.00)	(3.30, 4.50)	$-0.0500 \pm 0.0460 \pm 0.0104$	$0.1531 \pm 0.0838 \pm 0.0320$
(12.00, 30.00)	(2.10, 3.00)	$-0.0012 \pm 0.0222 \pm 0.0050$	$0.0453 \pm 0.0762 \pm 0.0300$
(12.00, 30.00)	(3.00, 3.30)	$0.0421 \pm 0.0416 \pm 0.0162$	$-0.0934 \pm 0.1377 \pm 0.0493$
(12.00, 30.00)	(3.30, 4.50)	$0.0537 \pm 0.0447 \pm 0.0124$	$0.3173 \pm 0.1411 \pm 0.0655$

Table 10
Values of the production asymmetries in bins of p_{T}, integrated over y, for B^+ and B^0 mesons for data collected in proton–proton collisions at the centre-of-mass energy of 7 TeV. The first uncertainties are statistical and the second systematic. The uncertainties among the bins are correlated due to the external inputs: $A_{CP}(B^+ \to J/\psi\, K^+)$ and $A_{\mathrm{D}}(\overline{K}^0)$ for $A_{\mathrm{P}}(B^+)$, and $|q/p|$ for $A_{\mathrm{P}}(B^0)$.

p_{T} [GeV/c]	$A_{\mathrm{P}}(B^+)_{\sqrt{s}=7\ \mathrm{TeV}}$	$A_{\mathrm{P}}(B^0)_{\sqrt{s}=7\ \mathrm{TeV}}$
(0.00, 2.00)	$0.0015 \pm 0.0067 \pm 0.0036$	$0.0215 \pm 0.0297 \pm 0.0025$
(2.00, 4.50)	$-0.0050 \pm 0.0040 \pm 0.0037$	$0.0123 \pm 0.0163 \pm 0.0078$
(4.50, 7.00)	$-0.0010 \pm 0.0045 \pm 0.0038$	$0.0124 \pm 0.0150 \pm 0.0042$
(7.00, 8.25)	$0.0083 \pm 0.0080 \pm 0.0041$	$-0.0440 \pm 0.0219 \pm 0.0012$
(8.25, 9.50)	$-0.0078 \pm 0.0096 \pm 0.0039$	$-0.0476 \pm 0.0248 \pm 0.0038$
(9.50, 10.75)	$-0.0220 \pm 0.0114 \pm 0.0044$	$0.0155 \pm 0.0297 \pm 0.0056$
(10.75, 12.00)	$-0.0045 \pm 0.0138 \pm 0.0043$	$0.0404 \pm 0.0357 \pm 0.0040$
(12.00, 15.00)	$0.0107 \pm 0.0124 \pm 0.0053$	$-0.0050 \pm 0.0269 \pm 0.0035$
(15.00, 30.00)	$-0.0146 \pm 0.0150 \pm 0.0065$	$0.0333 \pm 0.0298 \pm 0.0077$

Table 11
Values of the production asymmetries in bins of y, integrated over p_{T}, for B^+ and B^0 mesons for data collected in proton–proton collisions at the centre-of-mass energy of 7 TeV. The first uncertainties are statistical and the second systematic. The uncertainties among the bins are correlated due to the external inputs: $A_{CP}(B^+ \to J/\psi\, K^+)$ and $A_{\mathrm{D}}(\overline{K}^0)$ for $A_{\mathrm{P}}(B^+)$, and $|q/p|$ for $A_{\mathrm{P}}(B^0)$.

y	$A_{\mathrm{P}}(B^+)_{\sqrt{s}=7\ \mathrm{TeV}}$	$A_{\mathrm{P}}(B^0)_{\sqrt{s}=7\ \mathrm{TeV}}$
(2.10, 2.70)	$0.0007 \pm 0.0047 \pm 0.0036$	$0.0488 \pm 0.0205 \pm 0.0017$
(2.70, 2.85)	$-0.0131 \pm 0.0064 \pm 0.0036$	$-0.0366 \pm 0.0232 \pm 0.0027$
(2.85, 3.00)	$-0.0063 \pm 0.0061 \pm 0.0037$	$-0.0251 \pm 0.0213 \pm 0.0010$
(3.00, 3.15)	$-0.0125 \pm 0.0061 \pm 0.0039$	$-0.0478 \pm 0.0203 \pm 0.0017$
(3.15, 3.30)	$-0.0009 \pm 0.0063 \pm 0.0039$	$-0.0130 \pm 0.0203 \pm 0.0018$
(3.30, 3.70)	$-0.0060 \pm 0.0044 \pm 0.0043$	$-0.0143 \pm 0.0133 \pm 0.0017$
(3.70, 4.50)	$0.0041 \pm 0.0062 \pm 0.0046$	$0.0044 \pm 0.0173 \pm 0.0045$

Table 12
Values of the production asymmetries in bins of p_{T}, integrated over y, for B^+ and B^0 mesons for data collected in proton–proton collisions at the centre-of-mass energy of 8 TeV. The first uncertainties are statistical and the second systematic. The uncertainties among the bins are correlated due to the external inputs: $A_{CP}(B^+ \to J/\psi\, K^+)$ and $A_{\mathrm{D}}(\overline{K}^0)$ for $A_{\mathrm{P}}(B^+)$, and $|q/p|$ for $A_{\mathrm{P}}(B^0)$.

p_{T} [GeV/c]	$A_{\mathrm{P}}(B^+)_{\sqrt{s}=8\ \mathrm{TeV}}$	$A_{\mathrm{P}}(B^0)_{\sqrt{s}=8\ \mathrm{TeV}}$
(0.00, 2.00)	$-0.0105 \pm 0.0045 \pm 0.0031$	$0.0065 \pm 0.0230 \pm 0.0017$
(2.00, 4.50)	$-0.0033 \pm 0.0026 \pm 0.0031$	$-0.0188 \pm 0.0103 \pm 0.0009$
(4.50, 7.00)	$-0.0093 \pm 0.0029 \pm 0.0032$	$-0.0111 \pm 0.0092 \pm 0.0011$
(7.00, 8.25)	$-0.0094 \pm 0.0051 \pm 0.0033$	$-0.0192 \pm 0.0141 \pm 0.0015$
(8.25, 9.50)	$-0.0126 \pm 0.0061 \pm 0.0033$	$0.0015 \pm 0.0155 \pm 0.0009$
(9.50, 10.75)	$-0.0073 \pm 0.0073 \pm 0.0034$	$-0.0156 \pm 0.0177 \pm 0.0013$
(10.75, 12.00)	$0.0036 \pm 0.0090 \pm 0.0034$	$0.0017 \pm 0.0210 \pm 0.0027$
(12.00, 15.00)	$-0.0082 \pm 0.0079 \pm 0.0035$	$-0.0270 \pm 0.0171 \pm 0.0009$
(15.00, 30.00)	$-0.0251 \pm 0.0095 \pm 0.0040$	$0.0137 \pm 0.0177 \pm 0.0009$

Table 13
Values of the production asymmetries in bins of y, integrated over p_T, for B^+ and B^0 mesons for data collected in proton–proton collisions at the centre-of-mass energy of 8 TeV. The first uncertainties are statistical and the second systematic. The uncertainties among the bins are correlated due to the external inputs: $A_{CP}(B^+ \to J/\psi K^+)$ and $A_\mathrm{D}(\overline{K}^0)$ for $A_\mathrm{P}(B^+)$, and $\lvert q/p\rvert$ for $A_\mathrm{P}(B^0)$.

y	$A_\mathrm{P}(B^+)_{\sqrt{s}=8\ \mathrm{TeV}}$	$A_\mathrm{P}(B^0)_{\sqrt{s}=8\ \mathrm{TeV}}$
(2.10, 2.70)	$-0.0023 \pm 0.0029 \pm 0.0031$	$-0.0082 \pm 0.0128 \pm 0.0012$
(2.70, 2.85)	$-0.0080 \pm 0.0041 \pm 0.0031$	$-0.0237 \pm 0.0173 \pm 0.0009$
(2.85, 3.00)	$0.0003 \pm 0.0040 \pm 0.0032$	$0.0148 \pm 0.0159 \pm 0.0015$
(3.00, 3.15)	$-0.0038 \pm 0.0040 \pm 0.0032$	$-0.0140 \pm 0.0151 \pm 0.0009$
(3.15, 3.30)	$-0.0123 \pm 0.0042 \pm 0.0034$	$-0.0193 \pm 0.0158 \pm 0.0021$
(3.30, 3.70)	$-0.0138 \pm 0.0030 \pm 0.0034$	$-0.0029 \pm 0.0103 \pm 0.0010$
(3.70, 4.50)	$-0.0144 \pm 0.0042 \pm 0.0037$	$-0.0201 \pm 0.0137 \pm 0.0010$

Table 14
Values of the production asymmetries in bins of p_T, integrated over y, for the B^0_s meson and the Λ^0_b baryon for data collected in proton–proton collisions at the centre-of-mass energy of 7 TeV. The first uncertainties are statistical and the second systematic. The uncertainties among the bins are correlated due to the external inputs: $A_{CP}(B^+ \to J/\psi K^+)$, $A_\mathrm{D}(\overline{K}^0)$, $\lvert q/p\rvert_{B^0}$ and $\lvert q/p\rvert_{B^0_s}$ for $A_\mathrm{P}(\Lambda^0_b)$, and $\lvert q/p\rvert_{B^0_s}$ for $A_\mathrm{P}(B^0_s)$.

p_T [GeV/c]	$A_\mathrm{P}(B^0_s)_{\sqrt{s}=7\ \mathrm{TeV}}$	$A_\mathrm{P}(\Lambda^0_b)_{\sqrt{s}=7\ \mathrm{TeV}}$
(2.0, 7.0)	$-0.0166 \pm 0.0393 \pm 0.0082$	$-0.0130 \pm 0.0311 \pm 0.0133$
(7.0, 9.5)	$0.0247 \pm 0.0334 \pm 0.0050$	$0.0948 \pm 0.0476 \pm 0.0211$
(9.5, 12.0)	$0.0566 \pm 0.0349 \pm 0.0096$	$-0.0596 \pm 0.0722 \pm 0.0262$
(12.0, 30.0)	$-0.0382 \pm 0.0273 \pm 0.0054$	$-0.0146 \pm 0.0985 \pm 0.0369$

Table 15
Values of the production asymmetries in bins of y, integrated over p_T, for the B^0_s meson and the Λ^0_b baryon for data collected in proton–proton collisions at the centre-of-mass energy of 7 TeV. The first uncertainties are statistical and the second systematic. The uncertainties among the bins are correlated due to the external inputs: $A_{CP}(B^+ \to J/\psi K^+)$, $A_\mathrm{D}(\overline{K}^0)$, $\lvert q/p\rvert_{B^0}$ and $\lvert q/p\rvert_{B^0_s}$ for $A_\mathrm{P}(\Lambda^0_b)$, and $\lvert q/p\rvert_{B^0_s}$ for $A_\mathrm{P}(B^0_s)$.

y	$A_\mathrm{P}(B^0_s)_{\sqrt{s}=7\ \mathrm{TeV}}$	$A_\mathrm{P}(\Lambda^0_b)_{\sqrt{s}=7\ \mathrm{TeV}}$
(2.1, 3.0)	$0.0151 \pm 0.0445 \pm 0.0088$	$-0.0511 \pm 0.0399 \pm 0.0168$
(3.0, 3.3)	$0.0296 \pm 0.0566 \pm 0.0111$	$0.0514 \pm 0.0448 \pm 0.0171$
(3.3, 4.5)	$-0.0554 \pm 0.0432 \pm 0.0101$	$0.0638 \pm 0.0348 \pm 0.0160$

Table 16
Values of the production asymmetries in bins of p_T, integrated over y, for the B^0_s meson and the Λ^0_b baryon for data collected in proton–proton collisions at the centre-of-mass energy of 8 TeV. The first uncertainties are statistical and the second systematic. The uncertainties among the bins are correlated, due to the external inputs: $A_{CP}(B^+ \to J/\psi K^+)$, $A_\mathrm{D}(\overline{K}^0)$, $\lvert q/p\rvert_{B^0}$ and $\lvert q/p\rvert_{B^0_s}$, for $A_\mathrm{P}(\Lambda^0_b)$ and $\lvert q/p\rvert_{B^0_s}$ for $A_\mathrm{P}(B^0_s)$.

p_T [GeV/c]	$A_\mathrm{P}(B^0_s)_{\sqrt{s}=8\ \mathrm{TeV}}$	$A_\mathrm{P}(\Lambda^0_b)_{\sqrt{s}=8\ \mathrm{TeV}}$
(2.0, 7.0)	$0.0235 \pm 0.0264 \pm 0.0083$	$0.0292 \pm 0.0200 \pm 0.0096$
(7.0, 9.5)	$0.0257 \pm 0.0223 \pm 0.0049$	$0.0367 \pm 0.0302 \pm 0.0127$
(9.5, 12.0)	$-0.0286 \pm 0.0230 \pm 0.0053$	$0.0442 \pm 0.0437 \pm 0.0164$
(12.0, 30.0)	$0.0187 \pm 0.0186 \pm 0.0049$	$0.0902 \pm 0.0612 \pm 0.0253$

Table 17
Values of the production asymmetries in bins of y, integrated over p_T, for the B^0_s meson and the Λ^0_b baryon for data collected in proton–proton collisions at the centre-of-mass energy of 8 TeV. The first uncertainties are statistical and the second systematic. The uncertainties among the bins are correlated, due to the external inputs: $A_{CP}(B^+ \to J/\psi K^+)$, $A_\mathrm{D}(\overline{K}^0)$, $\lvert q/p\rvert_{B^0}$ and $\lvert q/p\rvert_{B^0_s}$, for $A_\mathrm{P}(\Lambda^0_b)$ and $\lvert q/p\rvert_{B^0_s}$ for $A_\mathrm{P}(B^0_s)$.

y	$A_\mathrm{P}(B^0_s)_{\sqrt{s}=8\ \mathrm{TeV}}$	$A_\mathrm{P}(\Lambda^0_b)_{\sqrt{s}=8\ \mathrm{TeV}}$
(2.1, 3.0)	$0.0364 \pm 0.0290 \pm 0.0103$	$0.0028 \pm 0.0247 \pm 0.0107$
(3.0, 3.3)	$-0.0078 \pm 0.0413 \pm 0.0063$	$0.0792 \pm 0.0317 \pm 0.0138$
(3.3, 4.5)	$0.0055 \pm 0.0298 \pm 0.0070$	$0.0682 \pm 0.0242 \pm 0.0142$

References

[1] M. Chaichian, A. Fridman, On a possibility for measuring effects of CP violation at pp colliders, Phys. Lett. B 298 (1993) 218.

[2] E. Norrbin, R. Vogt, Bottom production asymmetries at the LHC, arXiv:hep-ph/0003056.

[3] E. Norrbin, T. Sjöstrand, Production and hadronization of heavy quarks, Eur. Phys. J. C 17 (2000) 137, arXiv:hep-ph/0005110.

[4] T. Sjöstrand, S. Mrenna, P. Skands, A brief introduction to PYTHIA 8.1, Comput. Phys. Commun. 178 (2008) 852, arXiv:0710.3820.

[5] M. Bahr, et al., Herwig++ physics and manual, Eur. Phys. J. C 58 (2008) 639, arXiv:0803.0883.

[6] LHCb collaboration, R. Aaij, et al., Measurement of the $\overline{B}^0$–B^0 and $\overline{B}^0_s$–B^0_s production asymmetries in pp collisions at $\sqrt{s} = 7$ TeV, Phys. Lett. B 739 (2014) 218, arXiv:1408.0275.

[7] LHCb collaboration, R. Aaij, et al., Measurement of the $D^{\pm}$ production asymmetry in 7 TeV pp collisions, Phys. Lett. B 718 (2013) 902, arXiv:1210.4112.

[8] LHCb collaboration, R. Aaij, et al., Measurement of the D^+_s–D^-_s production asymmetry in 7 TeV pp collisions, Phys. Lett. B 713 (2012) 186, arXiv:1205.0897.

[9] LHCb collaboration, R. Aaij, et al., Study of the productions of Λ^0_b and $\overline{B}^0$ hadrons in pp collisions and first measurement of the $\Lambda^0_b \to J/\psi\, pK^-$ branching fraction, Chin. Phys. C 40 (2016) 011001, arXiv:1509.00292.

[10] LHCb collaboration, A.A. Alves Jr., et al., The LHCb detector at the LHC, J. Instrum. 3 (2008) S08005.

[11] R. Aaij, et al., The LHCb trigger and its performance in 2011, J. Instrum. 8 (2013) P04022, arXiv:1211.3055.

[12] V.V. Gligorov, M. Williams, Efficient, reliable and fast high-level triggering using a bonsai boosted decision tree, J. Instrum. 8 (2013) P02013, arXiv:1210.6861.

[13] T. Sjöstrand, S. Mrenna, P. Skands, PYTHIA 6.4 physics and manual, J. High Energy Phys. 05 (2006) 026, arXiv:hep-ph/0603175.

[14] I. Belyaev, et al., Handling of the generation of primary events in Gauss, the LHCb simulation framework, J. Phys. Conf. Ser. 331 (2011) 032047.

[15] D.J. Lange, The EvtGen particle decay simulation package, Nucl. Instrum. Methods A 462 (2001) 152.

[16] P. Golonka, Z. Was, PHOTOS Monte Carlo: a precision tool for QED corrections in Z and W decays, Eur. Phys. J. C 45 (2006) 97, arXiv:hep-ph/0506026.

[17] Geant4 collaboration, J. Allison, et al., Geant4 developments and applications, IEEE Trans. Nucl. Sci. 53 (2006) 270.

[18] Geant4 collaboration, S. Agostinelli, et al., Geant4: a simulation toolkit, Nucl. Instrum. Methods A 506 (2003) 250.

[19] M. Clemencic, et al., The LHCb simulation application, Gauss: design, evolution and experience, J. Phys. Conf. Ser. 331 (2011) 032023.

[20] LHCb collaboration, R. Aaij, et al., Measurement of CP asymmetry in $D^0 \to K^-K^+$ and $D^0 \to \pi^-\pi^+$ decays, J. High Energy Phys. 07 (2014) 041, arXiv:1405.2797.

[21] D0 Collaboration, V.M. Abazov, et al., Measurement of direct CP violation parameters in $B^{\pm} \to J/\psi K^{\pm}$ and $B^{\pm} \to J/\psi \pi^{\pm}$ decays with 10.4 fb^{-1} of Tevatron data, Phys. Rev. Lett. 110 (2013) 241801, arXiv:1304.1655.

[22] Belle Collaboration, K. Sakai, et al., Search for CP violating charge asymmetry in $B^{\pm} \to J/\psi K^{\pm}$ decays, Phys. Rev. D 82 (2010) 091104, arXiv:1008.2567.

[23] BaBar Collaboration, B. Aubert, et al., Measurement of branching fractions and charge asymmetries for exclusive B decays to charmonium, Phys. Rev. Lett. 94 (2005) 141801, arXiv:hep-ex/0412062.

[24] LHCb collaboration, R. Aaij, et al., Measurement of the $B^{\pm}$ production asymmetry and the CP-violating asymmetry in the decay $B^{\pm} \to J/\psi K^{\pm}$, Phys. Rev. D 95 (5) (2017) 052005, arXiv:1701.05501.

[25] M. Pivk, F.R. Le, Diberder, sPlot: A statistical tool to unfold data distributions, Nucl. Instrum. Methods A 555 (2005) 356, arXiv:physics/0402083.

[26] LHCb collaboration, R. Aaij, et al., Measurement of the fragmentation fraction ratio f_s/f_d and its dependence on B meson kinematics, J. High Energy Phys. 04 (2013) 001, arXiv:1301.5286.

[27] LHCb collaboration, R. Aaij, et al., Study of the kinematic dependences of Λ^0_b production in pp collisions and a measurement of the $\Lambda^0_b \to \Lambda^+_c \pi^-$ branching fraction, J. High Energy Phys. 08 (2014) 143, arXiv:1405.6842.

[28] L. Breiman, J.H. Friedman, R.A. Olshen, C.J. Stone, Classification and Regression Trees, Wadsworth International Group, Belmont, California, USA, 1984.

[29] B.P. Roe, et al., Boosted decision trees as an alternative to artificial neural networks for particle identification, Nucl. Instrum. Methods A 543 (2005) 577, arXiv:physics/0408124.

[30] K.S. Cranmer, Kernel estimation in high-energy physics, Comput. Phys. Commun. 136 (2001) 198, arXiv:hep-ex/0011057.

[31] Particle Data Group, C. Patrignani, et al., Review of particle physics, Chin. Phys. C 40 (2016) 100001.

[32] LHCb collaboration, R. Aaij, et al., Measurement of CP violation parameters and polarisation fractions in $B^0_s \to J/\psi\, \overline{K}^{*0}$ decays, J. High Energy Phys. 11 (2015) 082, arXiv:1509.00400.

[33] Heavy Flavor Averaging Group, Y. Amhis, et al., Averages of b-hadron, c-hadron, and τ-lepton properties as of summer 2016, arXiv:1612.07233, updated results and plots available at http://www.slac.stanford.edu/xorg/hfag/.

LHCb Collaboration

R. Aaij[40], B. Adeva[39], M. Adinolfi[48], Z. Ajaltouni[5], S. Akar[59], J. Albrecht[10], F. Alessio[40], M. Alexander[53], S. Ali[43], G. Alkhazov[31], P. Alvarez Cartelle[55], A.A. Alves Jr[59], S. Amato[2], S. Amerio[23], Y. Amhis[7], L. An[3], L. Anderlini[18], G. Andreassi[41], M. Andreotti[17,7], J.E. Andrews[60], R.B. Appleby[56], F. Archilli[43], P. d'Argent[12], J. Arnau Romeu[6], A. Artamonov[37], M. Artuso[61], E. Aslanides[6], G. Auriemma[26], M. Baalouch[5], I. Babuschkin[56], S. Bachmann[12], J.J. Back[50], A. Badalov[38], C. Baesso[62], S. Baker[55], V. Balagura[7,3], W. Baldini[17], R.J. Barlow[56], C. Barschel[40], S. Barsuk[7], W. Barter[56], F. Baryshnikov[32], M. Baszczyk[27,12], V. Batozskaya[29], B. Batsukh[61], V. Battista[41], A. Bay[41], L. Beaucourt[4], J. Beddow[53], F. Bedeschi[24], I. Bediaga[1], A. Beiter[61], L.J. Bel[43], V. Bellee[41], N. Belloli[21,9], K. Belous[37], I. Belyaev[32], E. Ben-Haim[8], G. Bencivenni[19], S. Benson[43], A. Berezhnoy[33], R. Bernet[42], A. Bertolin[23], C. Betancourt[42], F. Betti[15], M.-O. Bettler[40], M. van Beuzekom[43], Ia. Bezshyiko[42], S. Bifani[47], P. Billoir[8], T. Bird[56], A. Birnkraut[10], A. Bitadze[56], A. Bizzeti[18,21], T. Blake[50], F. Blanc[41], J. Blouw[11,†], S. Blusk[61], V. Bocci[26], T. Boettcher[58], A. Bondar[36,23], N. Bondar[31,40], W. Bonivento[16], I. Bordyuzhin[32], A. Borgheresi[21,9], S. Borghi[56], M. Borisyak[35], M. Borsato[39], F. Bossu[7], M. Boubdir[9], T.J.V. Bowcock[54], E. Bowen[42], C. Bozzi[17,40], S. Braun[12], M. Britsch[12], T. Britton[61], J. Brodzicka[56], E. Buchanan[48], C. Burr[56], A. Bursche[2], J. Buytaert[40], S. Cadeddu[16], R. Calabrese[17,7], M. Calvi[21,9], M. Calvo Gomez[38,13], A. Camboni[38], P. Campana[19], D.H. Campora Perez[40], L. Capriotti[56], A. Carbone[15,5], G. Carboni[25,10], R. Cardinale[20,8], A. Cardini[16], P. Carniti[21,9], L. Carson[52], K. Carvalho Akiba[2], G. Casse[54], L. Cassina[21,9], L. Castillo Garcia[41], M. Cattaneo[40], G. Cavallero[20], R. Cenci[24,20], D. Chamont[7], M. Charles[8], Ph. Charpentier[40], G. Chatzikonstantinidis[47], M. Chefdeville[4], S. Chen[56], S.F. Cheung[57], V. Chobanova[39], M. Chrzaszcz[42,27], X. Cid Vidal[39], G. Ciezarek[43], P.E.L. Clarke[52], M. Clemencic[40], H.V. Cliff[49], J. Closier[40], V. Coco[59], J. Cogan[6], E. Cogneras[5], V. Cogoni[16,40,6], L. Cojocariu[30], P. Collins[40], A. Comerma-Montells[12], A. Contu[40], A. Cook[48], G. Coombs[40], S. Coquereau[38], G. Corti[40], M. Corvo[17,7], C.M. Costa Sobral[50], B. Couturier[40], G.A. Cowan[52], D.C. Craik[52], A. Crocombe[50], M. Cruz Torres[62], S. Cunliffe[55], R. Currie[55], C. D'Ambrosio[40], F. Da Cunha Marinho[2], E. Dall'Occo[43], J. Dalseno[48], P.N.Y. David[43], A. Davis[3], K. De Bruyn[6], S. De Capua[56], M. De Cian[12], J.M. De Miranda[1], L. De Paula[2], M. De Serio[14,4], P. De Simone[19], C.T. Dean[53], D. Decamp[4], M. Deckenhoff[10], L. Del Buono[8], M. Demmer[10], A. Dendek[28], D. Derkach[35], O. Deschamps[5], F. Dettori[40], B. Dey[22], A. Di Canto[40], H. Dijkstra[40], F. Dordei[40], M. Dorigo[41], A. Dosil Suárez[39], A. Dovbnya[45], K. Dreimanis[54], L. Dufour[43], G. Dujany[56], K. Dungs[40], P. Durante[40], R. Dzhelyadin[37], A. Dziurda[40], A. Dzyuba[31], N. Déléage[4], S. Easo[51], M. Ebert[52], U. Egede[55], V. Egorychev[32], S. Eidelman[36,23], S. Eisenhardt[52], U. Eitschberger[10], R. Ekelhof[10], L. Eklund[53], S. Ely[61], S. Esen[12], H.M. Evans[49], T. Evans[57], A. Falabella[15], N. Farley[47], S. Farry[54], R. Fay[54], D. Fazzini[21,9], D. Ferguson[52], A. Fernandez Prieto[39], F. Ferrari[15,40], F. Ferreira Rodrigues[2], M. Ferro-Luzzi[40], S. Filippov[34], R.A. Fini[14], M. Fiore[17,7], M. Fiorini[17,7], M. Firlej[28], C. Fitzpatrick[41], T. Fiutowski[28], F. Fleuret[7,2], K. Fohl[40], M. Fontana[16,40], F. Fontanelli[20,8], D.C. Forshaw[61], R. Forty[40], V. Franco Lima[54], M. Frank[40], C. Frei[40], J. Fu[22,17], W. Funk[40], E. Furfaro[25,10], C. Färber[40], A. Gallas Torreira[39], D. Galli[15,5], S. Gallorini[23], S. Gambetta[52], M. Gandelman[2], P. Gandini[57], Y. Gao[3], L.M. Garcia Martin[69], J. García Pardiñas[39], J. Garra Tico[49], L. Garrido[38], P.J. Garsed[49], D. Gascon[38], C. Gaspar[40], L. Gavardi[10], G. Gazzoni[5], D. Gerick[12], E. Gersabeck[12], M. Gersabeck[56], T. Gershon[50], Ph. Ghez[4], S. Gianì[41], V. Gibson[49], O.G. Girard[41], L. Giubega[30], K. Gizdov[52], V.V. Gligorov[8], D. Golubkov[32], A. Golutvin[55,40], A. Gomes[1,1], I.V. Gorelov[33], C. Gotti[21,9], R. Graciani Diaz[38], L.A. Granado Cardoso[40], E. Graugés[38], E. Graverini[42], G. Graziani[18], A. Grecu[30], R. Greim[9], P. Griffith[16], L. Grillo[21,40,9], B.R. Gruberg Cazon[57], O. Grünberg[67], E. Gushchin[34], Yu. Guz[37], T. Gys[40], C. Göbel[62], T. Hadavizadeh[57], C. Hadjivasiliou[5], G. Haefeli[41], C. Haen[40], S.C. Haines[49], B. Hamilton[60], X. Han[12], S. Hansmann-Menzemer[12], N. Harnew[57], S.T. Harnew[48], J. Harrison[56], M. Hatch[40], J. He[63], T. Head[41], A. Heister[9], K. Hennessy[54], P. Henrard[5], L. Henry[8], E. van Herwijnen[40], M. Heß[67], A. Hicheur[2], D. Hill[57], C. Hombach[56], P.H. Hopchev[41], W. Hulsbergen[43], T. Humair[55], M. Hushchyn[35], D. Hutchcroft[54], M. Idzik[28], P. Ilten[58], R. Jacobsson[40], A. Jaeger[12], J. Jalocha[57], E. Jans[43], A. Jawahery[60], F. Jiang[3], M. John[57], D. Johnson[40], C.R. Jones[49], C. Joram[40], B. Jost[40], N. Jurik[57], S. Kandybei[45], M. Karacson[40], J.M. Kariuki[48], S. Karodia[53], M. Kecke[12], M. Kelsey[61], M. Kenzie[49], T. Ketel[44], E. Khairullin[35], B. Khanji[12], C. Khurewathanakul[41], T. Kirn[9], S. Klaver[56], K. Klimaszewski[29], S. Koliiev[46], M. Kolpin[12], I. Komarov[41], R.F. Koopman[44], P. Koppenburg[43], A. Kosmyntseva[32], M. Kozeiha[5], L. Kravchuk[34], K. Kreplin[12], M. Kreps[50], P. Krokovny[36,23], F. Kruse[10], W. Krzemien[29], W. Kucewicz[27,12], M. Kucharczyk[27], V. Kudryavtsev[36,23], A.K. Kuonen[41], K. Kurek[29], T. Kvaratskheliya[32,40], D. Lacarrere[40], G. Lafferty[56], A. Lai[16], G. Lanfranchi[19], C. Langenbruch[9], T. Latham[50], C. Lazzeroni[47], R. Le Gac[6], J. van Leerdam[43], A. Leflat[33,40], J. Lefrançois[7], R. Lefèvre[5], F. Lemaitre[40], E. Lemos Cid[39], O. Leroy[6], T. Lesiak[27], B. Leverington[12], T. Li[3], Y. Li[7], T. Likhomanenko[35,68], R. Lindner[40], C. Linn[40], F. Lionetto[42], X. Liu[3], D. Loh[50], I. Longstaff[53], J.H. Lopes[2], D. Lucchesi[23,15], M. Lucio Martinez[39], H. Luo[52], A. Lupato[23], E. Luppi[17,7], O. Lupton[40], A. Lusiani[24], X. Lyu[63], F. Machefert[7], F. Maciuc[30], O. Maev[31], K. Maguire[56], S. Malde[57], A. Malinin[68], T. Maltsev[36], G. Manca[16,6], G. Mancinelli[6], P. Manning[61], J. Maratas[5,22], J.F. Marchand[4], U. Marconi[15], C. Marin Benito[38], M. Marinangeli[41], P. Marino[24,20], J. Marks[12], G. Martellotti[26], M. Martin[6], M. Martinelli[41], D. Martinez Santos[39], F. Martinez Vidal[69], D. Martins Tostes[2], L.M. Massacrier[7], A. Massafferri[1], R. Matev[40], A. Mathad[50], Z. Mathe[40], C. Matteuzzi[21], A. Mauri[42], E. Maurice[7,2], B. Maurin[41], A. Mazurov[47], M. McCann[55,40], A. McNab[56], R. McNulty[13], B. Meadows[59], F. Meier[10], M. Meissner[12], D. Melnychuk[29], M. Merk[43], A. Merli[22,17], E. Michielin[23], D.A. Milanes[66], M.-N. Minard[4], D.S. Mitzel[12], A. Mogini[8], J. Molina Rodriguez[1], I.A. Monroy[66], S. Monteil[5], M. Morandin[23], P. Morawski[28], A. Mordà[6], M.J. Morello[24,20], O. Morgunova[68], J. Moron[28], A.B. Morris[52], R. Mountain[61], F. Muheim[52], M. Mulder[43], M. Mussini[15], D. Müller[56], J. Müller[10], K. Müller[42], V. Müller[10], P. Naik[48], T. Nakada[41], R. Nandakumar[51], A. Nandi[57], I. Nasteva[2], M. Needham[52], N. Neri[22], S. Neubert[12], N. Neufeld[40], M. Neuner[12], T.D. Nguyen[41], C. Nguyen-Mau[41,14], S. Nieswand[9], R. Niet[10], N. Nikitin[33], T. Nikodem[12], A. Nogay[68], A. Novoselov[37], D.P. O'Hanlon[50], A. Oblakowska-Mucha[28], V. Obraztsov[37], S. Ogilvy[19], R. Oldeman[16,6], C.J.G. Onderwater[70], J.M. Otalora Goicochea[2], A. Otto[40], P. Owen[42], A. Oyanguren[69], P.R. Pais[41], A. Palano[14,4], M. Palutan[19], A. Papanestis[51], M. Pappagallo[14,4], L.L. Pappalardo[17,7], W. Parker[60],

C. Parkes[56], G. Passaleva[18], A. Pastore[14,4], G.D. Patel[54], M. Patel[55], C. Patrignani[15,5], A. Pearce[40], A. Pellegrino[43], G. Penso[26], M. Pepe Altarelli[40], S. Perazzini[40], P. Perret[5], L. Pescatore[41], K. Petridis[48], A. Petrolini[20,8], A. Petrov[68], M. Petruzzo[22,17], E. Picatoste Olloqui[38], B. Pietrzyk[4], M. Pikies[27], D. Pinci[26], A. Pistone[20], A. Piucci[12], V. Placinta[30], S. Playfer[52], M. Plo Casasus[39], T. Poikela[40], F. Polci[8], A. Poluektov[50,36], I. Polyakov[61], E. Polycarpo[2], G.J. Pomery[48], A. Popov[37], D. Popov[11,40], B. Popovici[30], S. Poslavskii[37], C. Potterat[2], E. Price[48], J.D. Price[54], J. Prisciandaro[39,40], A. Pritchard[54], C. Prouve[48], V. Pugatch[46], A. Puig Navarro[42], G. Punzi[24,16], W. Qian[50], R. Quagliani[7,48], B. Rachwal[27], J.H. Rademacker[48], M. Rama[24], M. Ramos Pernas[39], M.S. Rangel[2], I. Raniuk[45,†], F. Ratnikov[35], G. Raven[44], F. Redi[55], S. Reichert[10], A.C. dos Reis[1], C. Remon Alepuz[69], V. Renaudin[7], S. Ricciardi[51], S. Richards[48], M. Rihl[40], K. Rinnert[54], V. Rives Molina[38], P. Robbe[7,40], A.B. Rodrigues[1], E. Rodrigues[59], J.A. Rodriguez Lopez[66], P. Rodriguez Perez[56,†], A. Rogozhnikov[35], S. Roiser[40], A. Rollings[57], V. Romanovskiy[37], A. Romero Vidal[39], J.W. Ronayne[13], M. Rotondo[19], M.S. Rudolph[61], T. Ruf[40], P. Ruiz Valls[69], J.J. Saborido Silva[39], E. Sadykhov[32], N. Sagidova[31], B. Saitta[16,6], V. Salustino Guimaraes[1], C. Sanchez Mayordomo[69], B. Sanmartin Sedes[39], R. Santacesaria[26], C. Santamarina Rios[39], M. Santimaria[19], E. Santovetti[25,10], A. Sarti[19,11], C. Satriano[26,19], A. Satta[25], D.M. Saunders[48], D. Savrina[32,33], S. Schael[9], M. Schellenberg[10], M. Schiller[53], H. Schindler[40], M. Schlupp[10], M. Schmelling[11], T. Schmelzer[10], B. Schmidt[40], O. Schneider[41], A. Schopper[40], K. Schubert[10], M. Schubiger[41], M.-H. Schune[7], R. Schwemmer[40], B. Sciascia[19], A. Sciubba[26,11], A. Semennikov[32], A. Sergi[47], N. Serra[42], J. Serrano[6], L. Sestini[23], P. Seyfert[21], M. Shapkin[37], I. Shapoval[45], Y. Shcheglov[31], T. Shears[54], L. Shekhtman[36,23], V. Shevchenko[68], B.G. Siddi[17,40], R. Silva Coutinho[42], L. Silva de Oliveira[2], G. Simi[23,15], S. Simone[14,4], M. Sirendi[49], N. Skidmore[48], T. Skwarnicki[61], E. Smith[55], I.T. Smith[52], J. Smith[49], M. Smith[55], H. Snoek[43], I. Soares Lavra[1], M.D. Sokoloff[59], F.J.P. Soler[53], B. Souza De Paula[2], B. Spaan[10], P. Spradlin[53], S. Sridharan[40], F. Stagni[40], M. Stahl[12], S. Stahl[40], P. Stefko[41], S. Stefkova[55], O. Steinkamp[42], S. Stemmle[12], O. Stenyakin[37], H. Stevens[10], S. Stevenson[57], S. Stoica[30], S. Stone[61], B. Storaci[42], S. Stracka[24,16], M. Straticiuc[30], U. Straumann[42], L. Sun[64], W. Sutcliffe[55], K. Swientek[28], V. Syropoulos[44], M. Szczekowski[29], T. Szumlak[28], S. T'Jampens[4], A. Tayduganov[6], T. Tekampe[10], G. Tellarini[17,7], F. Teubert[40], E. Thomas[40], J. van Tilburg[43], M.J. Tilley[55], V. Tisserand[4], M. Tobin[41], S. Tolk[49], L. Tomassetti[17,7], D. Tonelli[40], S. Topp-Joergensen[57], F. Toriello[61], E. Tournefier[4], S. Tourneur[41], K. Trabelsi[41], M. Traill[53], M.T. Tran[41], M. Tresch[42], A. Trisovic[40], A. Tsaregorodtsev[6], P. Tsopelas[43], A. Tully[49], N. Tuning[43], A. Ukleja[29], A. Ustyuzhanin[35], U. Uwer[12], C. Vacca[16,6], V. Vagnoni[15,40], A. Valassi[40], S. Valat[40], G. Valenti[15], R. Vazquez Gomez[19], P. Vazquez Regueiro[39], S. Vecchi[17], M. van Veghel[43], J.J. Velthuis[48], M. Veltri[18,18], G. Veneziano[57], A. Venkateswaran[61], M. Vernet[5], M. Vesterinen[12], J.V. Viana Barbosa[40], B. Viaud[7], D. Vieira[63], M. Vieites Diaz[39], H. Viemann[67], X. Vilasis-Cardona[38,13], M. Vitti[49], V. Volkov[33], A. Vollhardt[42], B. Voneki[40], A. Vorobyev[31], V. Vorobyev[36,23], C. Voß[9], J.A. de Vries[43], C. Vázquez Sierra[39], R. Waldi[67], C. Wallace[50], R. Wallace[13], J. Walsh[24], J. Wang[61], D.R. Ward[49], H.M. Wark[54], N.K. Watson[47], D. Websdale[55], A. Weiden[42], M. Whitehead[40], J. Wicht[50], G. Wilkinson[57,40], M. Wilkinson[61], M. Williams[40], M.P. Williams[47], M. Williams[58], T. Williams[47], F.F. Wilson[51], J. Wimberley[60], J. Wishahi[10], W. Wislicki[29], M. Witek[27], G. Wormser[7], S.A. Wotton[49], K. Wraight[53], K. Wyllie[40], Y. Xie[65], Z. Xing[61], Z. Xu[4], Z. Yang[3], Y. Yao[61], H. Yin[65], J. Yu[65], X. Yuan[36,23], O. Yushchenko[37], K.A. Zarebski[47], M. Zavertyaev[11,3], L. Zhang[3], Y. Zhang[7], A. Zhelezov[12], Y. Zheng[63], X. Zhu[3], V. Zhukov[33], S. Zucchelli[15]

[1] *Centro Brasileiro de Pesquisas Físicas (CBPF), Rio de Janeiro, Brazil*
[2] *Universidade Federal do Rio de Janeiro (UFRJ), Rio de Janeiro, Brazil*
[3] *Center for High Energy Physics, Tsinghua University, Beijing, China*
[4] *LAPP, Université Savoie Mont-Blanc, CNRS/IN2P3, Annecy-Le-Vieux, France*
[5] *Clermont Université, Université Blaise Pascal, CNRS/IN2P3, LPC, Clermont-Ferrand, France*
[6] *CPPM, Aix-Marseille Université, CNRS/IN2P3, Marseille, France*
[7] *LAL, Université Paris-Sud, CNRS/IN2P3, Orsay, France*
[8] *LPNHE, Université Pierre et Marie Curie, Université Paris Diderot, CNRS/IN2P3, Paris, France*
[9] *I. Physikalisches Institut, RWTH Aachen University, Aachen, Germany*
[10] *Fakultät Physik, Technische Universität Dortmund, Dortmund, Germany*
[11] *Max-Planck-Institut für Kernphysik (MPIK), Heidelberg, Germany*
[12] *Physikalisches Institut, Ruprecht-Karls-Universität Heidelberg, Heidelberg, Germany*
[13] *School of Physics, University College Dublin, Dublin, Ireland*
[14] *Sezione INFN di Bari, Bari, Italy*
[15] *Sezione INFN di Bologna, Bologna, Italy*

[16] *Sezione INFN di Cagliari, Cagliari, Italy*
[17] *Sezione INFN di Ferrara, Ferrara, Italy*
[18] *Sezione INFN di Firenze, Firenze, Italy*
[19] *Laboratori Nazionali dell'INFN di Frascati, Frascati, Italy*
[20] *Sezione INFN di Genova, Genova, Italy*
[21] *Sezione INFN di Milano Bicocca, Milano, Italy*
[22] *Sezione INFN di Milano, Milano, Italy*
[23] *Sezione INFN di Padova, Padova, Italy*
[24] *Sezione INFN di Pisa, Pisa, Italy*
[25] *Sezione INFN di Roma Tor Vergata, Roma, Italy*
[26] *Sezione INFN di Roma La Sapienza, Roma, Italy*
[27] *Henryk Niewodniczanski Institute of Nuclear Physics Polish Academy of Sciences, Kraków, Poland*
[28] *AGH - University of Science and Technology, Faculty of Physics and Applied Computer Science, Kraków, Poland*
[29] *National Center for Nuclear Research (NCBJ), Warsaw, Poland*
[30] *Horia Hulubei National Institute of Physics and Nuclear Engineering, Bucharest-Magurele, Romania*
[31] *Petersburg Nuclear Physics Institute (PNPI), Gatchina, Russia*
[32] *Institute of Theoretical and Experimental Physics (ITEP), Moscow, Russia*
[33] *Institute of Nuclear Physics, Moscow State University (SINP MSU), Moscow, Russia*
[34] *Institute for Nuclear Research of the Russian Academy of Sciences (INR RAN), Moscow, Russia*
[35] *Yandex School of Data Analysis, Moscow, Russia*
[36] *Budker Institute of Nuclear Physics (SB RAS), Novosibirsk, Russia*
[37] *Institute for High Energy Physics (IHEP), Protvino, Russia*
[38] *ICCUB, Universitat de Barcelona, Barcelona, Spain*
[39] *Universidad de Santiago de Compostela, Santiago de Compostela, Spain*
[40] *European Organization for Nuclear Research (CERN), Geneva, Switzerland*
[41] *Institute of Physics, Ecole Polytechnique Fédérale de Lausanne (EPFL), Lausanne, Switzerland*
[42] *Physik-Institut, Universität Zürich, Zürich, Switzerland*
[43] *Nikhef National Institute for Subatomic Physics, Amsterdam, The Netherlands*
[44] *Nikhef National Institute for Subatomic Physics and VU University Amsterdam, Amsterdam, The Netherlands*
[45] *NSC Kharkiv Institute of Physics and Technology (NSC KIPT), Kharkiv, Ukraine*
[46] *Institute for Nuclear Research of the National Academy of Sciences (KINR), Kyiv, Ukraine*
[47] *University of Birmingham, Birmingham, United Kingdom*
[48] *H.H. Wills Physics Laboratory, University of Bristol, Bristol, United Kingdom*
[49] *Cavendish Laboratory, University of Cambridge, Cambridge, United Kingdom*
[50] *Department of Physics, University of Warwick, Coventry, United Kingdom*
[51] *STFC Rutherford Appleton Laboratory, Didcot, United Kingdom*
[52] *School of Physics and Astronomy, University of Edinburgh, Edinburgh, United Kingdom*
[53] *School of Physics and Astronomy, University of Glasgow, Glasgow, United Kingdom*
[54] *Oliver Lodge Laboratory, University of Liverpool, Liverpool, United Kingdom*
[55] *Imperial College London, London, United Kingdom*
[56] *School of Physics and Astronomy, University of Manchester, Manchester, United Kingdom*
[57] *Department of Physics, University of Oxford, Oxford, United Kingdom*
[58] *Massachusetts Institute of Technology, Cambridge, MA, United States*
[59] *University of Cincinnati, Cincinnati, OH, United States*
[60] *University of Maryland, College Park, MD, United States*
[61] *Syracuse University, Syracuse, NY, United States*
[62] *Pontifícia Universidade Católica do Rio de Janeiro (PUC-Rio), Rio de Janeiro, Brazil* [24]
[63] *University of Chinese Academy of Sciences, Beijing, China* [25]
[64] *School of Physics and Technology, Wuhan University, Wuhan, China* [25]
[65] *Institute of Particle Physics, Central China Normal University, Wuhan, Hubei, China* [25]
[66] *Departamento de Fisica, Universidad Nacional de Colombia, Bogota, Colombia* [26]
[67] *Institut für Physik, Universität Rostock, Rostock, Germany* [27]
[68] *National Research Centre Kurchatov Institute, Moscow, Russia* [28]
[69] *Instituto de Fisica Corpuscular, Centro Mixto Universidad de Valencia – CSIC, Valencia, Spain* [29]
[70] *Van Swinderen Institute, University of Groningen, Groningen, The Netherlands* [30]

E-mail address: carbone@bo.infn.it (A. Carbone).

[1] Universidade Federal do Triângulo Mineiro (UFTM), Uberaba-MG, Brazil.
[2] Laboratoire Leprince-Ringuet, Palaiseau, France.
[3] P.N. Lebedev Physical Institute, Russian Academy of Science (LPI RAS), Moscow, Russia.
[4] Università di Bari, Bari, Italy.
[5] Università di Bologna, Bologna, Italy.
[6] Università di Cagliari, Cagliari, Italy.
[7] Università di Ferrara, Ferrara, Italy.
[8] Università di Genova, Genova, Italy.
[9] Università di Milano Bicocca, Milano, Italy.
[10] Università di Roma Tor Vergata, Roma, Italy.
[11] Università di Roma La Sapienza, Roma, Italy.
[12] AGH - University of Science and Technology, Faculty of Computer Science, Electronics and Telecommunications, Kraków, Poland.
[13] LIFAELS, La Salle, Universitat Ramon Llull, Barcelona, Spain.
[14] Hanoi University of Science, Hanoi, Viet Nam.
[15] Università di Padova, Padova, Italy.
[16] Università di Pisa, Pisa, Italy.
[17] Università degli Studi di Milano, Milano, Italy.
[18] Università di Urbino, Urbino, Italy.
[19] Università della Basilicata, Potenza, Italy.

[20] Scuola Normale Superiore, Pisa, Italy.
[21] Università di Modena e Reggio Emilia, Modena, Italy.
[22] Iligan Institute of Technology (IIT), Iligan, Philippines.
[23] Novosibirsk State University, Novosibirsk, Russia.
[24] Associated to Universidade Federal do Rio de Janeiro (UFRJ), Rio de Janeiro, Brazil.
[25] Associated to Center for High Energy Physics, Tsinghua University, Beijing, China.
[26] Associated to LPNHE, Université Pierre et Marie Curie, Université Paris Diderot, CNRS/IN2P3, Paris, France.
[27] Associated to Physikalisches Institut, Ruprecht-Karls-Universität Heidelberg, Heidelberg, Germany.
[28] Associated to Institute of Theoretical and Experimental Physics (ITEP), Moscow, Russia.
[29] Associated to ICCUB, Universitat de Barcelona, Barcelona, Spain.
[30] Associated to Nikhef National Institute for Subatomic Physics, Amsterdam, The Netherlands.
[†] Deceased.